Functional connectivity of the insula in the resting brain.

Functional connectivity of the insula in the resting brain

Franco Cauda [a,b,*], Federico D'Agata [a], Katiuscia Sacco [a], Sergio Duca [c], Giuliano Geminiani [b], Alessandro Vercelli [d]

[a] CCS fMRI, Koelliker Hospital, Turin, Italy
[b] Department of Psychology, University of Turin, Turin, Italy
[c] Department of Neuroscience, AOU San Giovanni Battista, Turin, Italy
[d] Department of Anatomy, Pharmacology and Forensic Medicine, National Institute of Neuroscience, Turin, Italy

ABSTRACT

The human insula is hidden in the depth of the cerebral hemisphere by the overlying frontal and temporal opercula, and consists of three cytoarchitectonically distinct regions: the anterior agranular area, posterior granular area, and the transitional dysgranular zone; each has distinct histochemical staining patterns and specific connectivity. Even though there are several studies reporting the functional connectivity of the insula with the cingulated cortex, its relationships with other brain areas remain elusive in humans. Therefore, we decided to use resting state functional connectivity to elucidate in details its connectivity, in terms of cortical and subcortical areas, and also of lateralization. We investigated correlations in BOLD fluctuations between specific regions of interest of the insula and other brain areas of right-handed healthy volunteers, on both sides of the brain. Our findings document two major complementary networks involving the ventral-anterior and dorsal-posterior insula: one network links the anterior insula to the middle and inferior temporal cortex and anterior cingulate cortex, and is primarily related to limbic regions which play a role in emotional aspects; the second links the middle-posterior insula to premotor, sensorimotor, supplementary motor and middle-posterior cingulate cortices, indicating a role for the insula in sensorimotor integration. The clear bipartition of the insula was confirmed by negative correlation analysis. Correlation maps are partially lateralized: the salience network, related to the ventral anterior insula, displays stronger connections with the anterior cingulate cortex on the right side, and with the frontal cortex on the left side; the posterior network has stronger connections with the superior temporal cortex and the occipital cortex on the right side. These results are in agreement with connectivity studies in primates, and support the use of resting state functional analysis to investigate connectivity in the living human brain.

Introduction

First described by anatomist J.C. Reil (1809), the human insular cortex (also known as the insula, Island of Reil, Brodmann areas 13 to 16) forms a distinct lobe located deep inside the lateral sulcus of the Sylvian fissure, and is hidden by the frontal and temporal opercula (Ture et al., 1999). Relative to that in the macaque, the insula is disproportionately increased in humans (Craig, 2008). Five to seven oblique gyri can be identified on the surface of the insula: these converge inferiorly, giving the appearance of the folds of a fan. A central insular sulcus, in which lies the main branch of the middle cerebral artery (Flynn et al., 1999), divides the lobe into an anterior and a posterior half.

Cytoarchitectonics and myeloarchitectonic can identify three major subdivisions in the insular cortex in humans and primates (Mesulam and Mufson, 1982a; Augustine, 1985; Türe et al., 1999; Bonthius et al., 2005), connected to the frontal, parietal, and temporal lobes, and especially to the cingulate gyrus (Augustine, 1996; Mesulam and Mufson, 1982a,b; Mufson and Mesulam, 1982; Vogt et al., 1987). Two of these, one antero-inferior and the other posterior, can be differentiated with histochemical staining for cytochrome oxidase, acetylcholinesterase and nicotinamide dinucleotide phosphate-diaphorase (Rivier and Clarke, 1997). The antero-inferior has a special relationship with rostral anterior cingulated cortex of Vogt (1993, 2004). The subdivisions of the insula also display different patterns of thalamic projections: for instance, in rhesus monkeys and in squirrel monkeys, the posterior subdivision receives a dense, coarse plexus of thalamic projections, that arise from the suprageniculate-limitans nucleus and fill all of layers IV to IIIa, whereas the thalamic projections to the middle field arise in the ventroposterior inferior

Abbreviations: BOLD, blood oxygen level-dependent; fMRI, functional magnetic resonance imaging; ROI, region of interest; rsFC, resting state functional connectivity; RSN, resting state networks; VOI, volume of interest.

* Corresponding author. Dipartimento di Psicologia, Via Po 14, 10123 Turin, Italy. Fax: +39 011 8146231.
E-mail address: franco.cauda@unito.it (F. Cauda).

nucleus, and form a finer plexus in layers IV and III (Jones and Burton, 1976).

The insula has been involved in processing visceral motor/sensory, gustatory, olfactory, vestibular/auditory, visual, verbal, pain, sensory/motor information, and inputs related to music and eating, and modulating attention and emotion; (Augustine, 1996; Brooks et al., 2005; Cole et al., 2006; Craig, 2002, 2003, 2004; Critchley et al., 2004; Devinsky et al., 1995; Lamm and Singer, 2010; Mutschler et al., 2009; Olausson et al., 2005; Ostrowsky et al., 2002; Pollatos et al., 2007; Schweinhardt et al., 2006). And finally, Flynn et al. (1999) have shown that the insula also participates in conditioned aversive learning, affective and motivational components of pain perception, mood stability, sleep, stress induced immunosuppression and language.

The advent of functional magnetic resonance imaging (fMRI) has enabled analyses of cortical connectivity in humans *in vivo*. In fact, spontaneous activity has been demonstrated with functional imaging techniques in various species. FMRI allows to visualize large-scale, spatial patterns of such intrinsic activity (Biswal et al., 1995; Vincent et al., 2007). "Functional connectivity" (FC) highlights differences among correlational methods of inferring brain connectivity, and defines "the temporal correlations across cortical regions", which represent an index of brain function (Friston et al., 1993; Horwitz, 2003). The temporal correlation between fluctuations in different areas is then often taken as a measure of functional connectivity. The term "resting state" refers to the condition of an individual lying in the scanner in absence of stimuli or tasks. Spontaneous resting state fluctuations of the Blood Oxygen Level Dependent (BOLD) fMRI signals show patterns of synchronous activation/deactivation that are coherent within anatomically and functionally related areas of the brain (Damoiseaux et al., 2006; Fox et al., 2005; Greicius et al., 2003; Hampson et al., 2002; Vincent et al., 2007). Intrinsic functional brain connectivity, as revealed by low-frequency spontaneous fluctuations in the time courses of fMRI signals, has recently drawn much interest. Domains of correlated activity, often referred as resting state networks (RSNs), identified within the cerebral cortex, are related to specific types of sensory, motor and cognitive functions (Beckmann et al., 2005; Cauda et al., 2010b; Damoiseaux et al., 2006; see Fox and Raichle, 2007 for a review). Recently, this technique was further validated by showing very unlikely that RSNs are produced artifactually, by aliasing of cardiac and respiratory cycles; in fact, RSNs are localized in the gray matter and are likely related to ongoing neuronal activity (De Luca et al., 2006). Moreover, RSNs display changes in BOLD signals that are comparable to task-related ones, i.e. up to 3% are consistent across individuals, and are stable across repeated sessions (Damoiseaux et al., 2006).

In the present study we use resting state FC (rsFC) and seed-region of interest (ROIs) correlation analysis to investigate the correlations in BOLD fluctuations between specific ROIs of the insular cortex and those of other brain areas. We show that the anterior and the posterior insular areas belong to two distinct functional networks; in addition to confirming the functional connections of these two regions with the anterior and posterior cingulate cortex, respectively (Taylor et al., 2008), we provide for the first time a detailed description of their other connectivity and provide evidence for a lateralization in these networks.

Materials and methods

Subjects

Seventeen healthy right-handed volunteers (8 males; mean = 54 - years old; SD = 19.1 years), free of neurological or psychiatric disorders, not taking medications known to alter brain activity, and with no history of drug or alcohol abuse, participated in the study. Written informed consent was obtained from each subject, in accordance with the Declaration of Helsinki. The study was approved by our institutional committee of the University of Torino on ethical use of human subjects. All subjects received a neuropsychiatric assessment, performed by a neurologist (GG); any neurological disease was excluded. In particular, dementia and mild cognitive impairment (MCI) were excluded; the clinician's judgment was based on a structured interview with the patient and an informant (Clinical Dementia Rating scale, CDR) (Hughes et al., 1982), and on the Mini Mental State Examination (MMSE) (Folstein et al., 1975) in which all patients received a score greater than or equal to 24. Subjects were also evaluated using a neuropsychological battery for MCI assessment, including the Rey word list for immediate and delayed recall (Rey, 1958), the Novelli short story for learning and recall (Novelli et al., 1986a), Raven's colored matrices (Bingham et al., 1966), the trail making test A and B (Reitan, 1955), the Rey figure for copy and recall (Osterrieth, 1944), and tasks for semantic and phonemic fluency (Novelli et al., 1986b). The results did not show any case of deficit in cognitive functions.

Moreover, psychiatric symptoms and depression were excluded through both clinical examination and rating scales (Brief Psychiatric Rating Scale and Geriatric Depression Scale). An experienced neuroradiologist (SD) examined the structural MRI slices: neuroradiological signs of cerebral atrophy, hydrocephalus, tumors, demyelination and cerebrovascular disease were excluded.

Task and image acquisition

Subjects were instructed simply to keep their eyes closed, think of nothing in particular, and not to fall asleep. After the scanning session, participants were asked if they had fallen asleep during the scan, and data from subject with positive or doubtful answers were excluded from the study.

Images were gathered on a 1.5 T INTERA™ scanner (Philips Medical Systems) with a SENSE high-field, high resolution (MRIDC) head coil optimized for functional imaging. Resting state functional $T2^*$ weighted images were acquired using echoplanar (EPI) sequences, with a repetition time (TR) of 2000 ms, an echo time (TE) of 50 ms, and a 90° flip angle. The acquisition matrix was 64×64, with a 200 mm field of view (FoV). A total of 200 volumes were acquired, with each volume consisting of 19 axial slices, parallel to the anterior–posterior (AC–PC) commissure; slice thickness was 4.5 mm with a 0.5 mm gap. To reach a steady-state magnetization before acquiring the experimental data, two scans were added at the beginning of functional scanning: the data from these scans were discarded.

Within a single session for each participant, a set of three-dimensional high-resolution T_1-weighted structural images was acquired, using a Fast Field Echo (FFE) sequence, with a 25 ms TR, an ultra-short TE, and a 30° flip angle. The acquisition matrix was 256×256, and the FoV was 256 mm. The set consisted of 160 contiguous sagittal images covering the whole brain. In-plane resolution was 1 mm × 1 mm and slice thickness 1 mm ($1 \times 1 \times 1$ mm^3 voxels).

Data analysis

BOLD imaging data were analyzed using the BrainVoyager QX software (Brain Innovation, Maastricht, Holland). Functional images were pre-processed as follows to reduce artifacts (Miezin et al., 2000): i) slice scan time correction was performed using a sinc interpolation algorithm; ii) 3D motion correction was applied: using a trilinear interpolation algorithm, all volumes were spatially aligned to the first volume by rigid body transformations, and the roto-translation information was saved for subsequent elaborations; iii) spatial smoothing was performed using a Gaussian kernel of 8 mm FWHM; iv) temporal filtering (linear trend removals), and a band pass filter of 0.01–0.08 Hz, used to reduce cardiac and respiratory noise as in (Biswal et al., 1995; Greicius et al., 2003), showed that the 0.08–0.01 Hz frequency range had the greatest power in revealing the underlying connectivity (Achard et al., 2006; Biswal et al., 1995;

Fransson, 2006; Greicius et al., 2009; Hagmann et al., 2008; Vincent et al., 2007).

Pre-processing was followed by a series of steps to facilitate accurate anatomical localization of brain activity and inter-subject averaging. First, each subject's slice-based functional scan was co-registered on his/her 3D high-resolution structural scan. Second, the 3D structural data set of each subject was skull-stripped and transformed into Talairach space (Talairach and Tournoux, 1988): the cerebrum was translated and rotated into the anterior–posterior commissure plane and then the borders of the cerebrum were identified. Third, the volume time course of each subject was created in the subject-specific anatomic space. The Talairach transformation of the morphologic images was performed in two steps. The first step consisted of rotating the 3D data set of each subject to align it with the stereotactic axes. In the second step, the extreme points of the cerebrum were specified. These points were then used to scale the 3D data sets to the dimensions of the standard brain of the Talairach and Tournoux atlas using a piecewise affine and continuous transformation for each of the 12 defined subvolumes.

Intersubject coregistraton was performed at the cortex-level using a cortex-based high-resolution intersubject alignment (see Supplementary materials for further details). Only for group statistics the individual maps were projected onto the normalized volumetric image using volumetric anatomy.

Selection of ROIs

We decided to systematically re-explore the parcellation of the insular cortex (Augustine, 1996). Using a high-resolution intersubject cortex alignment (see supplementary materials for further details) we created a template with anatomical images from all subjects, and drew ten $5\times5\times5$ mm^3 cubic seed ROIs over each unilateral 3D renderized insular surface on the template; this was done in an equispaced fashion, taking into account previous anatomical and MR imaging studies (Naidich et al., 2004; Ture et al., 1999; Varnavas and Grand, 1999). Briefly, ten ROIs (1–10) were chosen in three different horizontal planes: ROIs 1 and 4 were in the anterior short insular gyrus, 5 and 8 were in the middle short insular gyrus, 2, 6 and 9 were in the posterior short insular gyrus, and 3, 7 and 10 were in the anterior long insular gyrus (Fig. 1 and Table 1) (see Supplementary materials for details).

Functional connectivity analysis

FC maps were computed according to Margulies et al. (2007). BOLD time courses were extracted from each ROI by averaging over voxels within each region. Several nuisance covariates were included in the analyses to reduce the effects of physiological processes such as fluctuations related to cardiac and respiratory cycles (Bandettini and Bullmore, 2008; Napadow et al., 2008), or to motion. To this aim, we included 9 additional covariates that modeled nuisance signals sampled from White Matter (WM), Cerebro-Spinal Fluid (CSF), Global Signal (GS) (Fox et al., 2009; Weissenbacher et al., 2009), as well as from 6 motion parameters (3 rotations and 3 translations as saved by the 3D motion correction). We derived the GS/WM/CSF nuisance signals averaging the time courses of the voxels in each subject's whole brain/WM/CSF masks. These masks are generated by the segmentation process of each subject's brain.

All seed-based predictors were z-normalized, and orthogonalized, to ensure that the time series for each ROI reflected its unique variance. To exclude the possibility that orthogonalization leads to an underestimation of FC, analyses were repeated with each insular subdivision in a separate regression model. Results were highly similar to those found

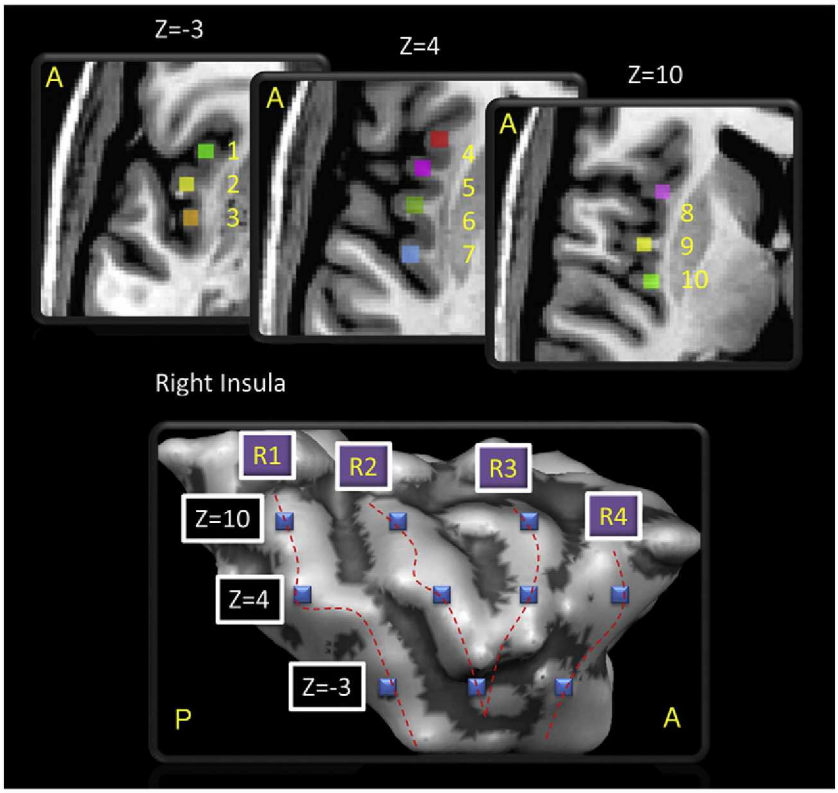

Fig. 1. Spatial distribution of the ROI used as seed regions for rsFC analyses. Ten equispaced $5\times5\times5$ mm^3 seed ROIs were drawn over the template's 3D renderized insular surface. The ROIs were chosen in three different horizontal planes (Z = −3, 4, 10), with ROIs 1 and 4 in the anterior short insular gyrus (R4), 5 and 8 in the middle short insular gyrus (R3), 2, 6 and 9 in the posterior short insular gyrus (R2), 3, 7 and 10 in the long insular gyrus (R1). Below a 3D-renderized lateral view of the right insula is shown. A = anterior, P = posterior.

Table 1
Talairach coordinates of the ROI used as seed regions for rsFC analyses.

ROI	X	Y	Z	mm^3
1 L	−34	12	−2.5	125
R	34	12	−2.5	125
2 L	−36	4.05	−2.5	125
R	38	5.05	−2.5	125
3 L	−36	−7.5	−2.5	125
R	38	−4.5	−2.5	125
4 L	−30	18	4.05	125
R	34	16	4.05	125
5 L	−32	9.05	4.05	125
R	36	7.05	4.05	125
6 L	−36	−0.5	4.05	125
R	38	0.05	4.05	125
7 L	−36	−9.5	4.05	125
R	38	−7.5	4.05	125
8 L	−30	9.05	10	125
R	32	9.05	10	125
9 L	−34	−1.5	10	125
R	34	−1.5	10	125
10 L	−34	−12	10	125
R	34	−10	10	125

The ROIs were in three different horizontal planes (Z = −3, 4, 10).
ROIs 1, 4 in the anterior short insular gyrus (R4); 5, 8 in the middle short insular gyrus (R3); 2, 6, 9 in the posterior short insular gyrus (R2); 3, 7, 10 in the long insular gyrus (R1).

with orthogonalization (Suppl. Fig. 1); therefore, only the orthogonalized results are presented here.

A correction (pre-whitening) for autocorrelation (Woolrich et al., 2001) was used.

For each seed ROI and for each subject a FC map was computed on a voxel-wise basis for each previously selected region. For each subject the general linear model (GLM) (Friston, 2007) for multiple regression analysis resulted in 10 ROI-based t-maps (SPMt) the statistical threshold of $p<0.05$ was corrected for multiple comparisons using the Bonferroni criterium ($p<0.05$, cluster threshold k>10 voxels in the native resolution).

Group statistical map

Random effect group-level analyses (RFX) were conducted using BrainVoyager QX 2.1 ($p<0.05$, cluster-level corrected using a Monte Carlo simulation (Forman et al., 1995; Goebel et al., 2006), see supporting online materials) for multiple comparisons (cluster threshold k>10 voxels in the native resolution). Fixed effect group-level analyses (FFX) were conducted using BrainVoyager QX 2.1 ($p<0.05$, Bonferroni corrected for multiple comparisons; cluster threshold k>10 voxels in the native resolution); resulting maps were projected on a 3D representation of the brain using the BrainVoyager QX cortical tool. Possible age or gender effects on the rsFC maps were examined using a correlational analysis between subject-specific ROI-generated maps, using the ANCOVA analysis tool implemented in BrainVoyager QX. For more details on methods see the supplementary online section.

Spatial probability maps

Spatial consistency of FC patterns across subjects was evaluated by computing probabilistic maps. This allows a sort of population-based analysis of the connectivity profile that would not be otherwise possible with fixed-effects group statistics. At each spatial location, such maps represent the relative number of subjects leading to significant task activity. In our study, for example, a 12% value would mean that 2 subjects activated the respective brain region. The probability map is calculated by summing voxel value of each ROI-generated network and dividing this value by the number of subjects. Single subject correlation maps before the probability maps creation were thresholded at $p<0.05$ Bonferroni-corrected, cluster dimension k>10 voxels in the native resolution.

ROI-based parcellation

K-means clustering

The idea behind functional connectivity-based parcellation is that voxels from the same functional region have resting signals that correlate in a similar and distinguishable manner with the remaining voxels in the brain. We used a methodology very similar to that described by Kim et al. (2009). For each of the 10 ROIs in the insula, we calculated a regression z(V), where V is the whole-brain set of gray matter voxels, resampled to a resolution $3\times3\times3\ mm^3$, and z represents the t maps obtained within the GLM model of the ROI's rsFC. The maps are stored in the rows of Z, the *functional connectivity profile matrix* of dimensions $10\times Nv$, where Nv is the number of gray matter voxels.

To describe the degree of similarity between functional connectivity maps, we computed the *functional similarity matrix* $S = 1/Nv(ZZ')$ which is the cross-correlation matrix of Z. Thus each element of this 10×10 matrix characterizes the degree of similarity between the correlation map $z_i(V)$ of ROI i and the correlation map $z_j(V)$ of the ROI j.

To cluster the ROIs in groups, we used the K-means cluster algorithm onto S, as by Kim et al. (2009); furthermore, we applied an unbiased procedure to choose the number of groups. Johansen-Berg et al. (2004) used a spectral reordering algorithm onto a similarity matrix (obtained from probabilistic tractography data, but containing similarity index of pairs of voxels as in our case) to find the reordering that minimizes the sum of element values multiplied by the squared distance of that element from the diagonal, hence forcing large values toward the diagonal (see Fig. 2 upper panel). If the data contain clusters (representing seed ROI with similar connectivity), then these clusters will be apparent in the reordered matrix and break points between clusters will represent locations where connectivity patterns change. A number of clusters were, on the basis of this reordered matrix, identified by visual inspection as groups of elements that were strongly correlated with each other and weakly correlated with the rest of the matrix.

To minimize the risk of inconsistent results obtained for the initial random placement of starting points, we computed the K-means 256 times, as recommended in Nanetti et al. (2009). The same three clusters were identified all 256 times. The process was also repeated with negative correlations, and the same results were obtained all 256 times.

Hierarchical clustering

We performed hierarchical clustering to map a dendrogram of our ROIwise clustering results. We employed Cluster 3.0 developed by Michael Eisen at Stanford University (http://bonsai.ims.u-tokyo.ac.jp/~mdehoon/software/cluster/software.htm) to perform the calculations and TreeView (http://jtreeview.sourceforge.net/) to map dendrograms. The similarity matrix S was built using the Euclidean Distance and Centroid Linkage as clustering method. In Centroid Linkage Clustering, a vector is assigned to each pseudo-item, and this vector is used to compute the distances between this pseudo-item and all remaining items or pseudo-items using the same similarity metric as was used to calculate the initial similarity matrix. The vector is the average of the vectors of all actual items contained within the pseudo-item. Thus, when a new branch of the tree is formed joining together a branch with n items and an actual item, the new pseudo-item is assigned a vector that is the average of the $n+1$ vectors it contains, and not the average of the two joined items.

Voxelwise parcellation

Fuzzy C-means clustering

We applied fuzzy clustering on unsmoothed insular parenchyma to achieve a voxelwise segregation of the underlying insular networks.

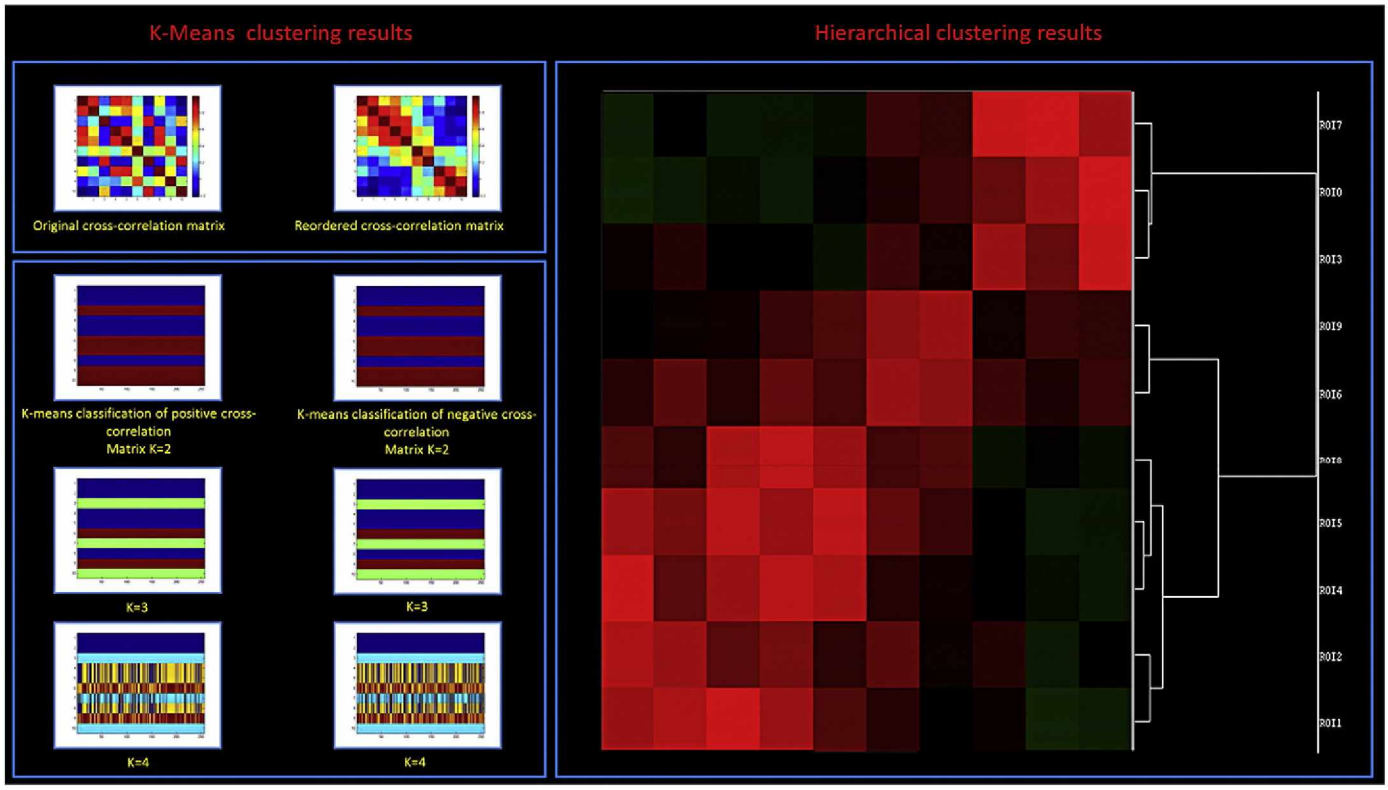

Fig. 2. Left upper panel: positive rsFC similarity matrix. Shows connectivity-based parcellation of Insula, original (Upper Left Panel) and reordered (Upper Right Panel) cross-correlation matrices, on the axis the ROI numbers. Left lower panel: K-means with varying clustering coefficents (K). Results for 256 K-means classification of positive (lower left panels) and negative (lower right panels) cross-correlation matrices, on the axis the ROI and the trials numbers. Right panel: dendrogram obtained with hierarchical clustering.

Insular gray matter meshes were segmented from each subject's morphological image and coregistered using a high-resolution inter-subject cortex alignment (see Supplementary Method section). Insular voxels were submitted to a voxelwise unsupervised fuzzy clustering technique.

Fuzzy clustering partitions a subset of n voxels in c "clusters" of activation (Smolders et al., 2007; Zadeh, 1977). The z-standardized signal time courses of all voxels are simultaneously considered, compared, and assigned to representative cluster time courses (cluster centroids). This data-driven method thus decomposes the original fMRI time series into a predefined number of spatiotemporal modes, which include a spatial map and an associated cluster centroid time course. The extent to which a voxel belongs to a cluster is defined by the similarity (as measured, e.g., by correlation) of its time course to the cluster centroid. In this method, "fuzziness" relates to the fact that a voxel is generally not uniquely assigned to one cluster, but, instead, the similarity of the voxel time course to each cluster centroid is determined. This is expressed by the "membership" u_{cn} of voxel n to cluster c. Cluster time course and membership functions are updated in an iterative procedure (Bezdek et al., 1984) that terminates when successive iterations do not further change memberships and cluster centers significantly as determined via classical cluster algorithm distance measures. For the current fMRI dataset, the number of clusters was fixed to 2 (see Supplementary Method section) and the fuzziness coefficient was set to 0.4. as suggested in literature (Fadili et al., 2000, 2001; Golay et al., 1998; Moller et al., 2002).We applied principal component analyses to the datasets to reduce dimensionality while capturing at least 90% of the total variance/covariance. Group cluster maps were obtained using probability maps. The resulting fuzzy clustering maps were reported in the interval [0–100%] and superimposed on the inflated representation of a template brain (average brain).

Hierarchical clustering

As shown in Fig. 2 (right panel). Examining the distance there are 3 predominant clusters:

I). ROIs 7, 10, 3
II). ROIs 9, 6
III). ROIs 8, 5, 4, 2, 1.

Clusters II and III were more similar (Transitional zone and Anterior Insula) than cluster I (Posterior Insula), but they split in two well before the other divisions (53% of total distance). Then cluster III split in two: ROIs 2, 1 and ROIs 8, 5, 4 (84% of total distance).

In summary, hierarchical clustering confirms our precedent K-means analysis adding more information on the similarity of the intermediate zone and suggesting a possible secondary division of the Anterior Insula cluster (also in the spectral analysis, although less clearly, the division can be evidenced, see Fig. 2 left panels).

Results

One subject was excluded from the analyses because of a movement that exceeded the limits subsequently indicated. No patients were reported having fallen asleep during the scanning. Thus the revised demographic of the subjects was as follows: sixteen right-handed healthy volunteers (8 males; mean = 53 years old; SD = 19 years). An ANCOVA correlational analysis between each subject-specific ROI-generated map by age and gender revealed no significant correlation among them ($q<0.05$ FDR (Genovese et al., 2002) corrected, cluster threshold $k>5$ voxels in the native resolution).

Spatial reliability of our data was assessed with the Spearman Brown split-half method (Charter, 2001), and showed a good-to-high reliability index (min 0.57, mean 0.69, max 0.79) (Suppl. Table 1).

Subject movement was assessed by summing the deviations (3 translations plus 3 rotations at a radius of 50 mm) used to compensate for head motion during image acquisition. Head movement, expressed in RMS mm, was averaged over subjects. This quantity was a mild 0.29 ± 0.09 mm (mean $\pm$ standard deviation) for the 16 subjects. The Pearson bivariate coefficient was calculated with for movement and age. The result was 0.09 ($p = 0.75$); based on this, we conclude that the ages of the subjects are unlikely to be correlated with the head movements in the MR scanner.

ROI-based parcellation

Since the insulae of both sides show the same parcellation, only right insular results are presented here.

Fig. 2 (upper left panel) shows three clusters in the reordered matrix for the positive correlation with the seed ROI:

1) ROIs 2, 1, 5, 4, 8;
2) ROIs 6, 9;
3) ROIs 3, 7, 10.

To confirm these results, we also applied the K-means (with $K = 3$) to the columns of the S matrix, thereby associating each ROI with one of three clusters, based on the similarity of their connectivity. To determine the reliability of the spectral reordering method in selecting the optimal number of clusters, we also calculated the K-means with $K = 2$ and $K = 4$. For positive and negative correlations, the following two clusters were always found with $K = 2$:

1) ROIs 1, 2, 4, 5, 8;
2) ROIs 3, 6, 7, 9, 10.

With $K = 4$, the stability of the clustering was lower (Fig. 2, lower panel) and we had the solution distribution shown in Suppl. Table 22.

Visual inspection of the results of the functional connectivity-based parcellation with $K = 3$ revealed two clearly delineated networks corresponding to cluster 1 (ROIs 1, 2, 4, 5, and 8) — hereafter called "Anterior Network" and to cluster 3 (ROIs 3, 7, 10) — hereafter called "Posterior Network". The intermediate cluster 2 (ROIs 6 and 9) shows a connectivity pattern that is positioned "in between" the other two clusters (Fig. 2); we interpret this as a transition area as also supported by subsequent analysis (Fuzzy clustering). Separate application of K-means clustering to the maps of correlated and anticorrelated areas led to the same results (Figs. 3 and 4), with an opposite polarity: the pattern anticorrelated with anterior insular area was similar to the positively correlated posterior area, and vice versa. Nevertheless, the anticorrelated maps were much less reproducible among subjects than were the positively correlated ones.

Voxelwise parcellation

We submitted each insular parenchyma to a voxelwise Fuzzy clustering algoritm. We ensured an optimal implementation of the Fuzzy clustering algorithm by performing an unsupervised search for the optimal number of clusters (see Supplementary Method section) leading to a number of two clusters. It is interesting to note that, unlike the ROI-based technique, the voxelwise clustering has divided the insula into only two clusters, plus an area where voxels show transitional characteristics.

Fig. 5 shows two clusters, one in the ventral-anterior and one in the dorsal-posterior in the insular parenchyma bilaterally, corresponding to the clusters 1 and 3 of the ROI-based parcellation. As suggested in literature (Fadili et al., 2000, 2001; Golay et al., 1998; Moller et al., 2002) we set the parameter "m" controlling the degree of fuzziness to a value within the range of values commonly used in FCM on fMRI datasets (0.4) that allows some voxels to be classified in more than one cluster: indeed, in between the two clusters we can recognize an area in which the voxels have a time course that can be interpreted either as cluster 1 or as a cluster 2. This area is roughly corresponding to the transitional area found with the ROI-based technique. Both insulae show the same ventral-anterior dorsal-posterior subdivision.

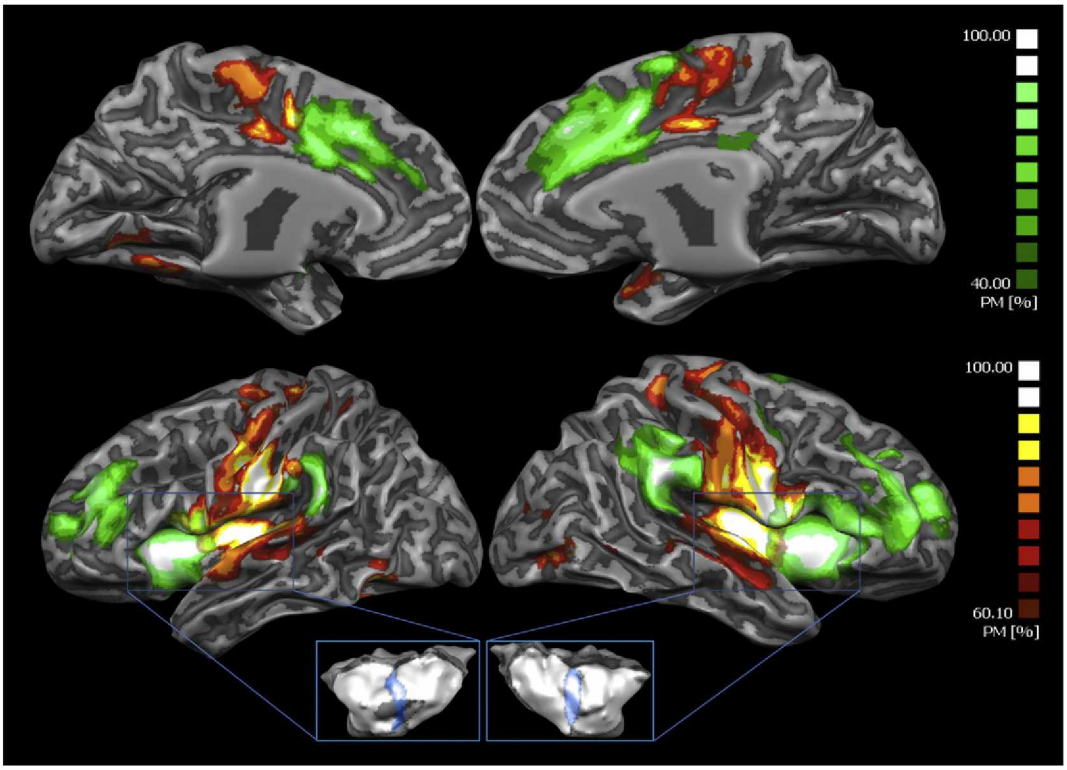

Fig. 3. Probability maps of correlated voxels for anterior and posterior patterns. Colors from green to white indicate an increasing spatial overlapping probability (%). Single subject correlation maps before the creation of probability maps are thresholded at $p < 0.05$ Bonferroni-corrected, with cluster dimension $k > 10$ voxels in the native resolution. Maps are projected on a 3D brain surface with the BrainVoyager QX surface tool.

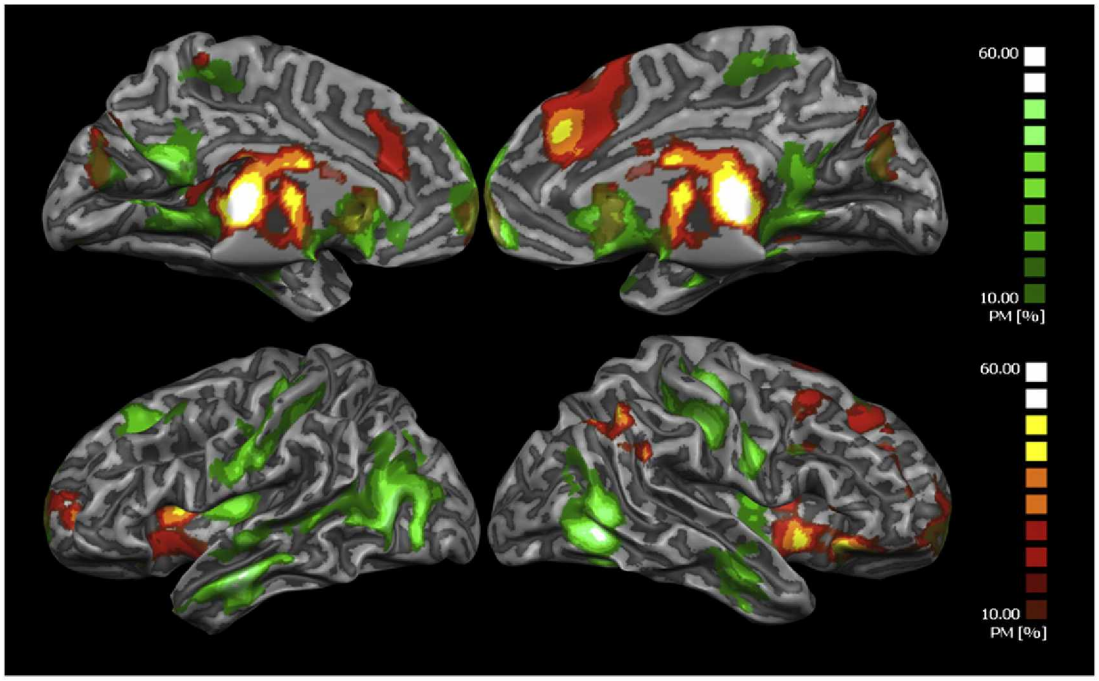

Fig. 4. Probability maps of anticorrelated voxels for anterior and posterior patterns. Colors from green to white indicate an increasing spatial overlapping probability (%). Single subject correlation maps before the creation of probability maps are thresholded at $p<0.05$ Bonferroni-corrected, with cluster dimension k>10 voxels in the native resolution. Maps are projected on a 3D brain surface with the BrainVoyager QX surface tool.

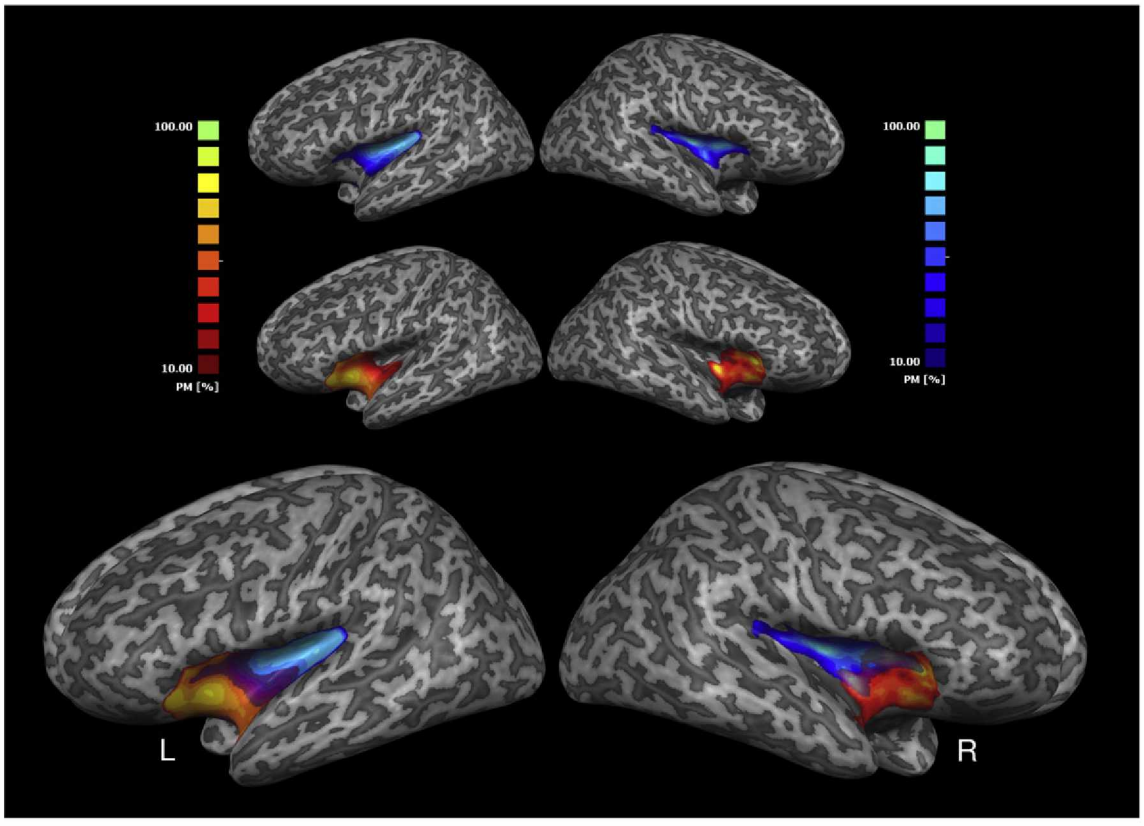

Fig. 5. Voxelwise clustering. Connectivity-based parcellation of human insular cortex. The figure shows the probabilities for each voxel in each insular GM layer to be classified in one of the two clusters generated by the fuzzy voxelwise C-means algorithm. The color scheme represents the probability of overlapping brains in each voxel across the 16 subjects. Maps are projected on an inflated 3D brain surface with the BrainVoyager QX surface tool. Upper panel: probabilistic map for posterior clusters. Colors from blue to green indicate an increasing spatial overlapping probability (%). Middle panel: probabilistic map for anterior clusters. Colors from red to green indicate an increasing spatial overlapping probability (%). Lower Panel: Joint probabilistic maps for both clusters.

Spatial probability maps

Probability maps computed for assessing the spatial consistency and reproducibility of seed-generated maps, yielded a high level of overlap among specific ROI-related rsFC maps for each subject (see Figs. 3 and 4).

Rostrocaudal and dorsoventral variations

In agreement with previous reports (see Discussion), we observed marked differences in connectivity along the anteroposterior axis: as the ROI was moved from rostral to caudal, the connectivity changed from an anterior pattern related to the ventralmost anterior insula, involving the middle and inferior frontal gyri, the rostral anterior cingulate cortex (rACC), to a dorsal-posterior visuo-sensorimotor network (posterior pattern), related to the temporoparietal cortex (mainly the supramarginal gyrus) and connected the middle-posterior insular cortex, involving the dorsoposterior cingulate cortex, the pre- and postcentral gyri, the superior temporal gyrus as well as some occipital areas.

As explained earlier we used functional connectivity-based parcellation, to classify the correlation maps. This classification procedure clearly assigns all the maps to one of the two groups; the exceptions are maps 6 and 9, which have an intermediate profile between the two patterns. The selected maps of all subjects, together with a GLM-fixed effect corrected for multiple comparisons, document the two well separated patterns shown in Figs. 5 and 6.

Examining the dorsoventral differences in connectivity we found that one of the two patterns was present through all the insular height and that both patterns coexisted in the middle-dorsal insula, the transitional area (Fig. 7).

Positively correlated networks

ROIs 1, 2, 4, 5 and 8 showed a bilateral pattern of connectivity (anterior pattern) involving the anterior insula, the superior, middle and inferior frontal gyri, the bilateral temporoparietal junction, the rACC, the cuneus, the precuneus as well as the superior temporal gyri (Figs. 3, 6, 7, Suppl. Figs. 2 and 3, Suppl. Tables 2, 3, 5, 6, 9). ROIs 3, 7 and 10 showed a bilateral pattern of connectivity (posterior pattern) that linked the sensorimotor, supplementary motor, superior temporal, middle temporal, lingual and cerebellar cortex (Figs. 3, 6, 7 Suppl. Figs. 2 and 3, Suppl. Tables 4, 8, 11). ROIs 6 and 9 showed a pattern that was transitional between the anterior and posterior ones (Figs. 3, 6, 7 Suppl.

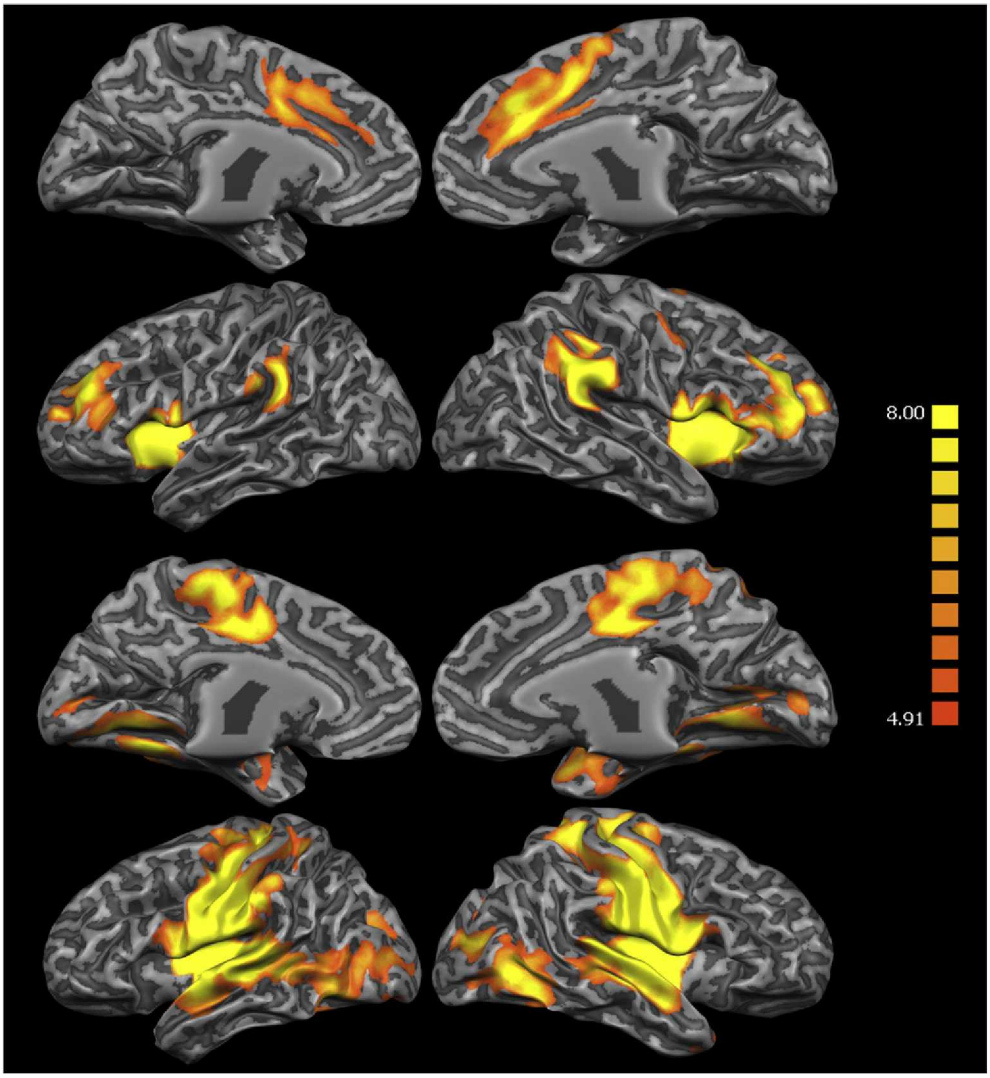

Fig. 6. rsFC correlations for anterior and posterior patterns. Fixed effect for all subjects, $p<0.05$ Bonferroni corrected for multiple comparisons, cluster threshold $k>10$ voxels. Colors from red to yellow indicate positively correlated voxels, upper part anterior, lower part posterior patterns. Maps projected on a 3D brain surface with the BrainVoyager QX surface tool.

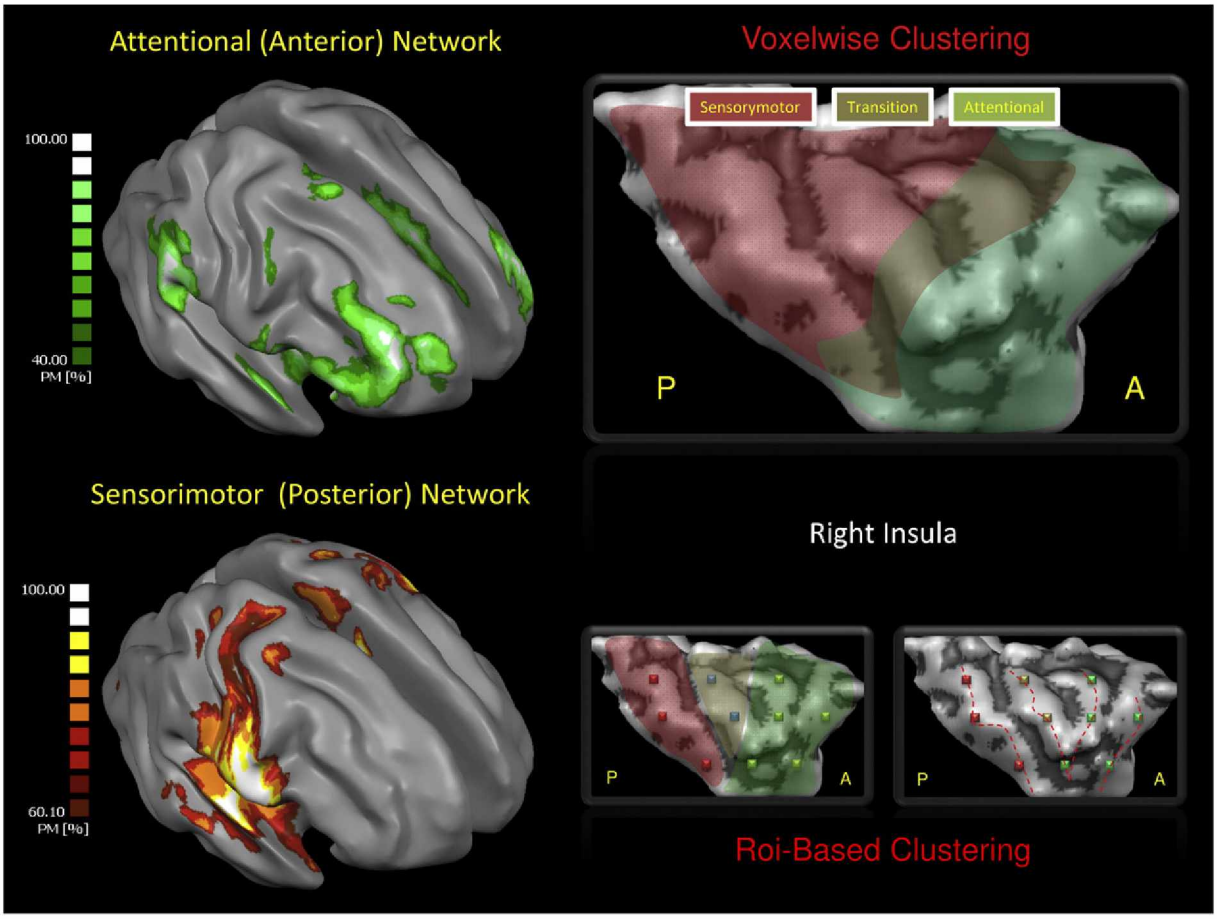

Fig. 7. Spatial distribution of anterior and posterior patterns. Colors from green to white indicate an increasing spatial overlapping probability (%). Single subject correlation maps before the probability maps creation are thresholded at $p<0.05$ Bonferroni-corrected, cluster dimension $k>10$ voxels in the native resolution. Maps are projected on a 3D brain surface with the BrainVoyager QX surface tool. The figure in between shows the spatial distribution of the two patterns on a lateral view of the right insula.

Figs. 2 and 3, Suppl. Tables 7 and 10). The Euclidean distances for the two different patterns for two sample ROIs of each pattern (5, 8 and 7, 10 respectively) showed that distances relative to anterior pattern are shorter than those for posterior pattern (Suppl. Fig. 5, Suppl. Results).

Anticorrelated networks

The pattern of negatively correlated networks was the reverse of the positively correlated ones: the salience detection pattern was mostly related to the caudal insula, whereas the visuo-sensory-motor pattern was related primarily to the anterior insula. The spatial subdivisions of the patterns of connectivity were rather inconstant, and were less topographically distinct than for the positive correlations (Figs. 4 and 7; Suppl. Fig. 4; Suppl. Tables 12–21). Nonetheless the clustering procedure applied on the pattern of negatively correlated networks led to the same results as for the positive pattern (see the connectivity-based parcellization results). Furthermore, the Euclidean distance was reversed with shorter connections for posterior anticorrelated network than for anterior anticorrelated network (Suppl. Fig. 5, Suppl. Results). Since the ROIs that show positive correlations for the salience pattern were also negatively correlated with the sensorimotor pattern, and vice-versa, we considered the possibility of two anticorrelated networks in the FC of the insula (Fox et al., 2005). This notion is supported by the change in the time course of the standardized BOLD signal. In fact, the two patterns were alternative to each other (Fig. 8 and Suppl. Fig. 6), showing that increases in the BOLD signal for one pattern corresponded to decreases in the other.

FFT power spectrum was calculated for the anterior and posterior insular clusters of one sample subject. The anterior insular power spectrum shows two peaks, at about 0.03 Hz and 0.06 Hz. The posterior insular power spectrum shows only the first one. The two time courses are anticorrelated, the Pearson product-moment correlation coefficient is $r=-0.47$.

The maximum phase shift between the two time courses is reached in a series of three peaks centered about 0.055 Hz, where the maximum cross coherence is also reached.

A conjunction analysis of spatial overlapping areas revealed that the some areas were shared between the anterior and posterior

Fig. 8. Time course analysis of one sample subject. In the upper part, spectrograms and FFT power spectrum were calculated for the anterior and posterior insular cluster. The anterior insular power spectrum shows two peaks, at about 0.03 Hz and 0.06 Hz. The posterior insular power spectrum shows only the peak centered at 0.03 Hz. In the lower part, the time courses of the two clusters are visualized together with the correlation between the two time series. The two time courses are anticorrelated, the Pearson product-moment correlation coefficient is $r=-0.47$. Over the time course panel, cross coherence and phase shift between the two insular time courses are visualized: the maximum phase shift between the two time courses is reached in a series of three peaks centered about 0.055 Hz. The maximum cross coherence is also centered at about 0.055 Hz. To obtain this figure the time courses of one sample subject were converted to an ASCII file and imported to the sigview software (sigview 1.9.9, http://www.sigview.com) for FFT-based analysis. The intensity data were pre-conditioned in sigview before FFT analysis by subtracting the mean from each data point, removing linear trends, removing any values greater than 2 standard deviations of the mean, and applying a Hanning window.

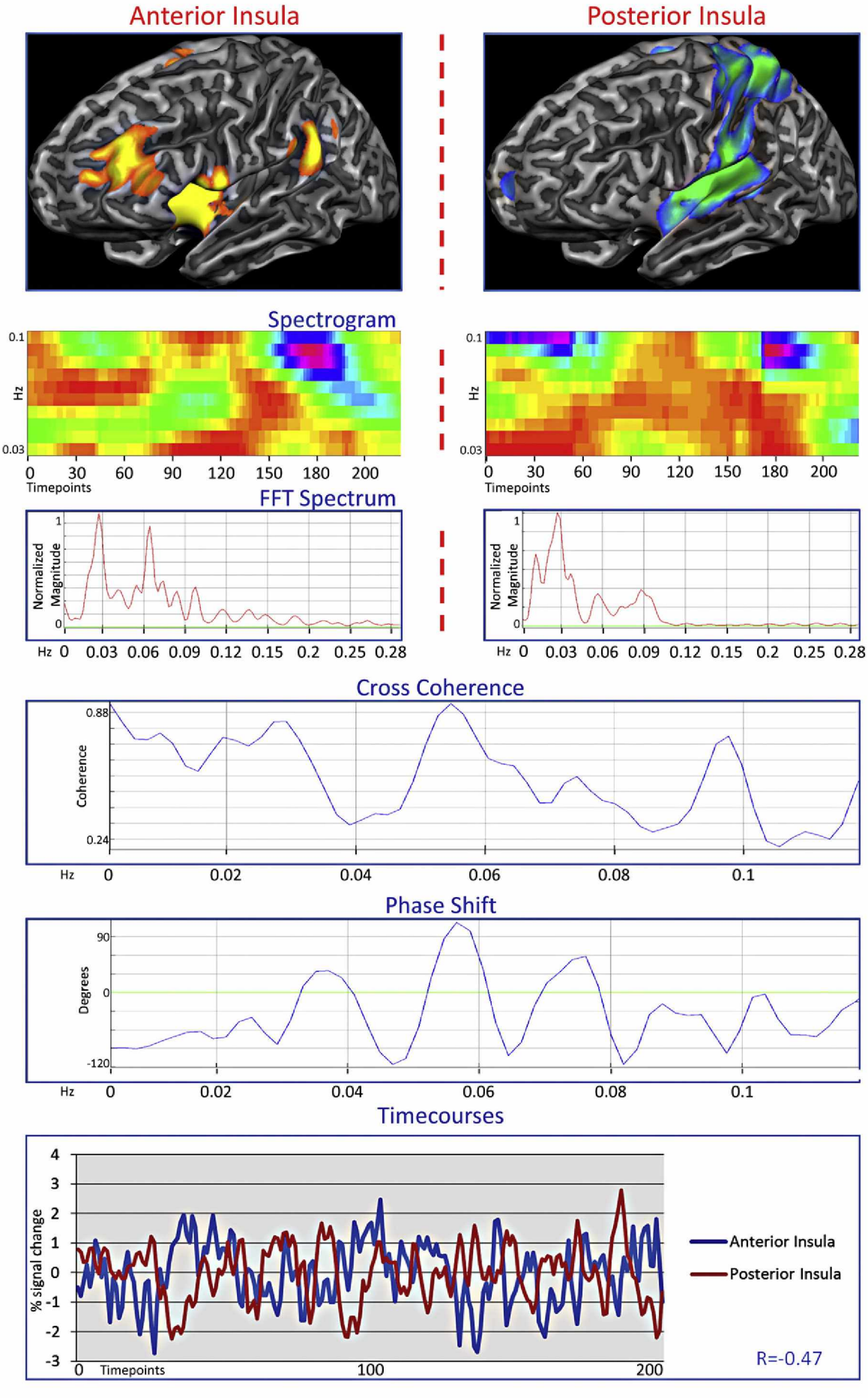
Anterior Insula
Posterior Insula
Spectrogram
0.1
Hz
0.03
0 30 60 90 120 150 180 200
Timepoints
FFT Spectrum
Normalized Magnitude
1
0
Hz 0 0.03 0.06 0.09 0.12 0.15 0.2 0.25 0.28
Cross Coherence
0.88
Coherence
0.24
Hz 0 0.02 0.04 0.06 0.08 0.1
Phase Shift
90
Degrees
0
-120
Hz 0 0.02 0.04 0.06 0.08 0.1
Timecourses
% signal change
4 3 2 1 0 -1 -2 -3
0 Timepoints 100 200
Anterior Insula
Posterior Insula
R=-0.47

Table 2
Subcortical connectivity.

ROI	Positive correlations	Negative correlations
1 L	Put	Put CauH CauB
R	Put SubTH GPM GPL, VA VL MD	Put CauH CauB
2 L	Put SN	Put CauT, Pul
R	Put GPM GPL SN SubTH, MD VA VL	Put
3 L	Put CauH CauB CauT GPL GPM SubTH	Put CauB CauT, MD AN VA Pul
R	Put SubTH CauH CauB, VL VPM MD	Put CauB CauT, MD AN VA Pul
4 L	Put Nac GPL, VL	CauH CauB
R	Put GPL GPM SubTH, VA VL MD	CauH CauB
5 L	Put GPM GPL SubTH SN, VA VL VPL VPM	–
R	Put GPL SubTH SN, VA VL MD	–
6 L	CauB Put GPM SN SubTH, VA VL VPL VPM	–
R	CauH CauB Put GPL SN SubTH, VA VL VPL VPM MD	–
7 L	Put	CauT CauB Put, Pul MDN
R	Put	CauT CauB, Pul MDN
8 L	Put GPL GPM, VPL VPM VL	CauB CauH
R	Put	CauB CauH
9 L	Put CauB GPM	CauH CauB
R	Put CauB GPL	CauH
10 L	Put	CauH CauB, MD Pul
R	Put	CauH CauB CauT SN, Pul MD VA SubTH

$p<0.05$ Bonferroni corrected for multiple comparisons, cluster threshold $k>10$ voxels. i) Basal ganglia: CauH, Caudate Head; CauB, Caudate Body; CauT, Caudate Tail; GPL, Globus Pallidus Lateral; GPM, Globus Pallidus Medial; NAc, Nucleus Accumbens; Put, Putamen; SN, Substantia Nigra; SubTH, Subthalamic Nucleus; ii) Thalamic nuclei: AN, Anterior Nucleus; MD, Medial Dorsal; Pul, Pulvinar; VA, Ventral Anterior; VL, Ventral Lateral; VPL, Ventral Posterior Lateral; VPM, Ventral Posterior Medial.

patterns (Suppl. Fig. 6): these included the left anterior insula and the left anterior cingulate gyrus, as well as the medial frontal gyri and the cunei of both sides. Applying winner-take-all maps, the posterior pattern was present in the sensorimotor, occipital, dorsolateral prefrontal, orbitofrontal, medial frontal, temporal polar and anterior cingulate cortices, while the anterior pattern was more prevalent in the rest of the brain (Suppl. Fig. 6).

Subcortical connectivity

Positive correlations (Table 2) with the basal ganglia and the thalamus were present in maps 1–6 and 8, with maximal correlations found in map 6. Conversely, no positive correlations for the thalamus, and only rare ones for the basal ganglia, were found in maps 7, 9 and 10. This was compatible with a dorso-ventral and a rostro-caudal gradient of decorrelation: the connections to subcortical structures were stronger in dorsal/rostral insular areas and decreased towards the ventral and caudal insula.

Limbic connectivity

The cingulate gyrus is almost always connected in positively correlated maps, except in map 10; the rostral anterior cingulate cortex is always connected as well, except in maps 2, 3, and 6. The parahippocampal gyri, the amygdala and the hippocampus are positively correlated in posterior maps 7, 9, and 10 (Suppl. Tables 2–11, Suppl. Fig. 2).

Cerebellar connectivity

Connectivity with cerebellar structures is found in almost all positively correlated maps except for maps 8 and 9 (Suppl. Tables 2–11, Suppl. Fig. 2).

Lateralization

As shown in Fig. 9, the right anterior ROIs are more connected with the brainstem, pons and the right thalamus, as well as with the left middle/posterior insula, the right dorsolateral prefrontal cortex, the right rostral anterior cingulate cortex and the right supramarginal gyrus. The left anterior ROIs show greater connectivity with the right posterior insula, the left dorsolateral prefrontal cortex, and bilaterally with the supplementary motor area. The right posterior ROIs have little connectivity with left posterior ROIs, while the left posterior ROI is more connected with the cuneus/lingual gyrus and the superior temporal gyrus on both sides, and with the right postcentral gyrus, the left thalamus and the left pre/postcentral gyrus. In inspecting this lateralization of the functionally connected cortical areas (Suppl. Figs. 7–10), we found that at this level the lateralization could discriminate between positively and negatively correlated maps and between A and B networks (see Suppl. Results).

Discussion

Even though there are several studies reporting the functional connectivity of the insula with the cingulated cortex, its relationships with other brain areas remain elusive in humans. Therefore, we decided to use rsFC to elucidate in details its connectivity, in terms of cortical and subcortical areas, and also of lateralization. The temporal correlation between slow fluctuations of intrinsic activity in different regions observed in this study relates to resting state, and cannot be used to infer the network involved in the execution of a specific task or the processing of specific stimuli. Resting state fMRI showed that the human insula is functionally involved in two distinct neural networks: i) the anterior pattern is related to the ventralmost anterior insula, and is connected to the rostral anterior cingulate cortex, the middle and inferior frontal cortex, and the temporoparietal cortex; ii) the posterior pattern is associated with the dorsal posterior insula, and is connected to the dorsal-posterior cingulate, sensorimotor, premotor, supplementary motor, temporal cortex, and to some occipital areas. The two neural networks likely subserve different functions: the first, emotional salience detection and attentional control-related pattern (Corbetta and Shulman, 2002; Dosenbach et al., 2006; Fox et al., 2006; Seeley et al., 2007), is mostly related to the integration of multiple cognitive, homeostatic and emotional (i.e. interoceptive) functions; the second to skeletomotor body orientation, environmental monitoring, and response selection (Flynn et al., 1999; Craig, 2002, 2008; Kurth et al., 2010a,b; Taylor et al., 2008). Enrollment of cortical sites in each of these neural networks seems to be mutually exclusive, since negatively correlated structures displayed a reversed pattern, compared to the positively correlated networks; moreover, the activation of single structures of either network was anticorrelated, thus reinforcing the idea that the anterior and posterior portions of the insula subserve different functions, and are connected to different networks that operate independently of one another. Finally, we document a certain degree of lateralization, which can be observed both in the positively and negatively correlated networks.

Methodological considerations, significance of resting state analysis, and detection of correlated/anticorrelated networks

In resting-state fMRI, all patterns result from random fluctuations. It can be argued that, even though one may discuss the sources (origin) and the coherence of these fluctuations, they remain random processes, e.g. their amplitude and phase are random variables. On the

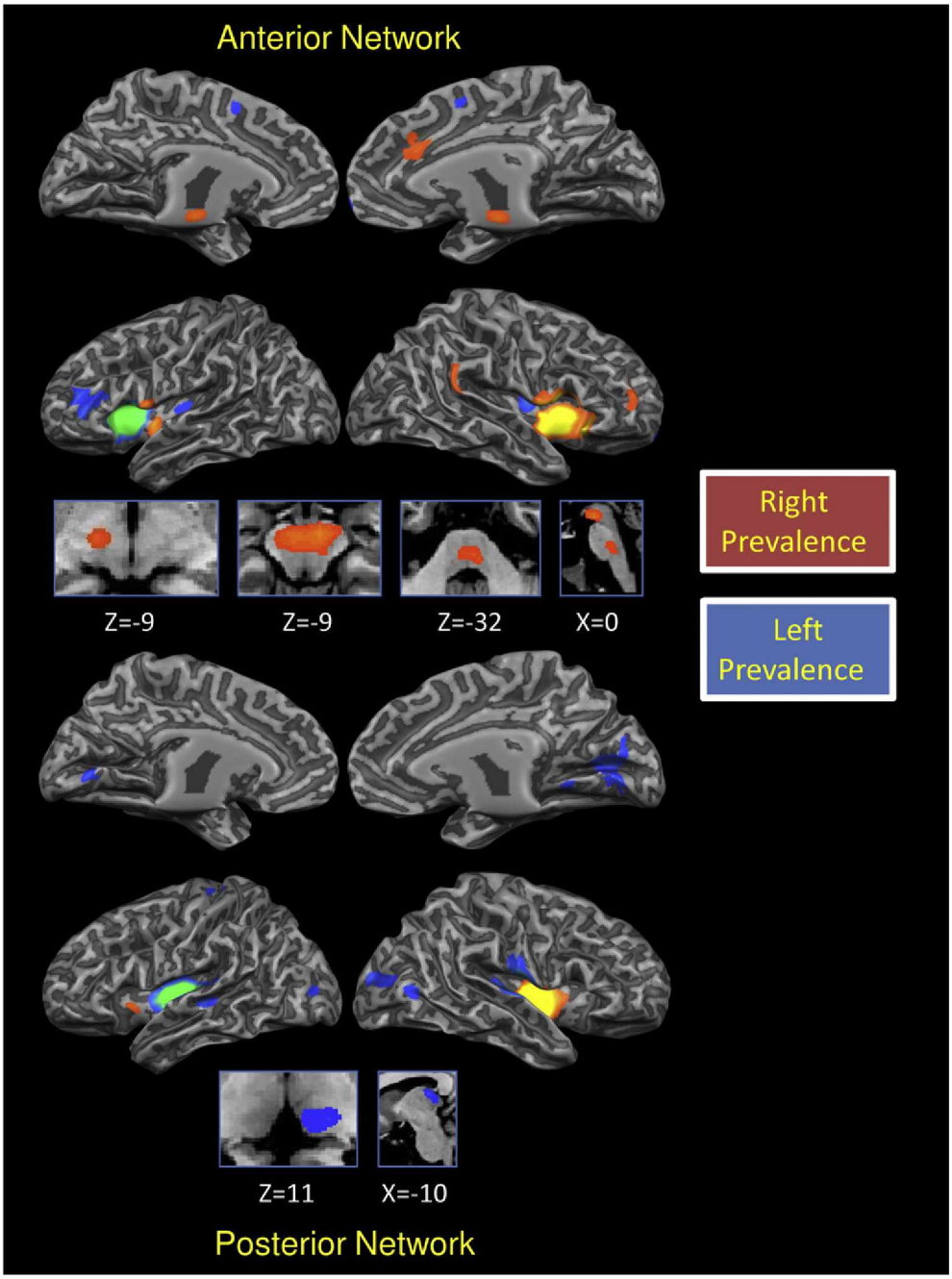

Fig. 9. Lateralization of unilateral ROIs placed in the local maxima of anterior and posterior patterns: right minus left ROI results. Two sample *t*-test, $p<0.05$ FDR corrected for multiple comparisons, cluster threshold K>10 voxels. Colors from red to yellow indicate right lateralized voxels. Colors from blue to green indicate left lateralized voxels. Maps are projected on a 3D brain surface with the BrainVoyager QX surface tool.

other hand, intrinsic connectivity networks detected by resting state analysis are highly reproducible across participants and scans, thus suggesting that the fluctuations reflect the existence of networks, and are driven by intrinsic activity events constrained by anatomy (Ghosh et al., 2008; Van Dijk et al., 2010). Recent studies have shown a high level of test–retest reliability (Shehzad et al., 2009).

Our sample is heterogeneous for age. Previous reports have shown that functional connectivity increases from childhood to adulthood (Fair et al., 2008: samples of 7–9 y. o. children vs. adults; Stevens et al., 2007: 12–30 y. o. subjects), but is decreased in elderly people (Damoiseaux, et al., 2008: >70 y. o. subjects). Therefore, we did not include children, adolescents or elderly people, ages at which connectivity changes. In addition, a random effect analysis controlling for age and gender effects, gave maps overall similar to those obtained with fixed effect analysis, even though less clear-cut (Suppl. Fig. 3). K-means clustering (K = 3) of the maps obtained with random effect analysis led to the same results as with fixed effect. In addition, at a behavioral level, we found no correlation between subject age and their head movements while in the scanner.

Since the size of our ROIs exceeds the average thickness of the cortex (3 mm), we cannot exclude that our ROIs may also include signal from adjacent structures. This can be further exasperated by smoothing. Conversely, inclusion of signals of WM and CSF as covariates reduces the chance of contamination. Indeed, additional analyses were conducted using alternative ROIs, i.e. ROIs which were moved from the original location in the dorsal, rostral and caudal directions (3 mm in each

direction), and reduced ($3\times3\times3$ mm^3) and increased ($8\times8\times8$ mm^3) in size. The resulting maps and those obtained using the original ROIs were very similar: probabilistic maps showed high overlapping between the original and the alternative connectivity maps (see Suppl. Fig. 11). This result indicates that, although possible, contamination is very unlikely.

Whereas physiological noise is correlated with rsFC patterns (Birn et al., 2006, 2008), the regression of nuisance correlations that can be estimated from the data (via white-matter, ventricular, and whole-brain signals) is sufficient to reduce artifacts associated with respiration and other sources of spurious noise (Van Dijk et al., 2010). Indeed, sophisticated statistical correction of both respiratory and heart rate results in only minor changes in correlations among default mode network regions (van Buuren et al., 2009).

These considerations, together with the high reproducibility of the two patterns across subjects (areas ascribed to one pattern were activated within the same pattern in 60–100% of the subjects), methods (see fuzzy clustering) and the high reliability of our results, lead us to excluded that the patterns result merely from random fluctuations, or from unintentional tasks by individual subjects. Moreover, our FC results are in agreement with anatomical data obtained in primates (see below).

The functional anticorrelation between the two major patterns for the anterior and posterior insula is in agreement with findings of other studies on the resting brain. In fact, two opposite sets of responses are commonly found during performance of cognitive tasks: one group of regions increases activity specifically, whereas another group decreases it (Fox et al., 2005). However, the value of anticorrelations in elucidating FC is debated (Fox et al., 2009; Weissenbacher et al., 2009), and these results should be interpreted with caution, particularly when mean signal intensity during the run is removed (Van Dijk et al., 2010).

Connectivity of insula in primates

The human insula is enlarged in size relative to that in primates, and consists of two distinct areas, one ventroanterior and the other dorsoposterior; these areas are characterized by specific histological features, and are separated by a transition zone (Mesulam and Mufson, 1982a). Recent studies report three different cytoarchitectonic areas in the human posterior insular cortex, two granular and one dysgranular, located ventroanteriorly (Kurth et al., 2010a,b). These data are in agreement with previous work, in which granularity was used to split the insula into three belt-like parts (Mesulam and Mufson, 1982a): the posterior dysgranular area identified recently corresponds to part of the classical dysgranular belt surrounding the inner/anterior agranular belt. We confirm the existence of a tripartition. On the other hand, it might be argued that the sparse 10-ROI grid, especially due to the use of relatively large ROIs, can hardly fit with cytoarchitectonic subdivisions. Nevertheless, voxelwise analysis, which is independent from ROI positioning, confirms the finding of two, one anteroventral and one posterodorsal, partitions.

Tract tracing studies in primates document that each of these areas is specifically connected to other cortical and subcortical regions. Recent functional neuroimaging techniques, resting state analysis, and diffusion tensor imaging in humans show striking similarities with anatomical connectivity reported for the primate (for detailed review see Flynn et al., 1999). Our results in the resting human brain are in agreement with the primate data, and confirm that the ventral anterior insula in humans is functionally connected to the anterior cingulate (ACC) and frontal cortices, whereas the dorsal posterior insula is linked to motor, somatosensory, and temporal cortices. The term ACC needs some clarification: based on morphological grounds and connectivity, Vogt (Vogt, 1993; Vogt et al., 2004) proposed to divide ACC in rostral and caudal parts, and to name the latter as midcingulate cortex. In our study the ventral anterior insula is linked to the rostral ACC of Vogt. Tract tracing studies in primates further show that the insula is connected to the primary and secondary somatosensory areas, to orbitofrontal, prefrontal and motor cortex, superior temporal gyrus, temporal pole, frontal operculum, parietal operculum, primary auditory and auditory association cortices, visual association cortex, olfactory bulb, anterior cingulate cortex, amygdaloid body, hippocampus and entorhinal cortex (Flynn et al., 1999). Most cortical connections of the insula are reciprocal and topographically organized (Aggleton et al., 1980).

Participation of the insula to default mode networks n rsFC

Resting state connectivity allows to characterize large scale networks without contamination from cognitive tasks. rsFC shows that the ventroanterior insula participates in a salience detection, attentional pattern (Corbetta and Shulman, 2002; Fox et al., 2006), involving the middle and inferior frontal gyri, the ACC as well as the temporoparietal cortex (mainly the supramarginal gyrus)., This salience network (SN) displays key nodes in the AI and ACC (Fox et al., 2006; Seeley et al., 2007) and serves to integrate sensory data with visceral, autonomic, and hedonic information. Seeley et al. (2007) and Menon and Uddin (2010) propose that this SN serves to identify the most homeostatically relevant among several internal and extrapersonal stimuli in order to guide behavior. Uddin and Menon (2009) hypothesized that the right AI could "act as a 'causal outflow hub' coordinating two large-scale networks important for mediating attention to the external (executive-control) and internal (default-mode) worlds" (Menon and Uddin, 2010).

We also demonstrate the existence of a middle-posterior network, i.e. a visuomotor pattern, which involves the dorsoposterior cingulate cortex, the pre and postcentral gyri, the superior temporal gyrus as well as some occipital areas connected with middle-posterior insular cortex — these areas are likely involved in skeletomotor body orientation, environmental monitoring, and response selection. Anatomical studies show that the posterior dorsal insula is mostly connected to the supplementary motor area, the somatosensory cortex, the auditory cortex, the inferior parietal lobule. These functions, and its connectivity, relate the posterior insula with another default-mode network including the ventromedial prefrontal cortex (VMPFC) and posterior cingulate cortex (PCC) (Cauda et al., 2010a; Fox et al., 2006; Seeley et al., 2007). Anatomical connections to the temporal lobe and cingulate regions have been demonstrated for the overall insula: nevertheless, the connections with the cingulate cortex are area-specific, since the anterior insula is mostly connected with the anterior cingulate cortex, whereas the posterior insula is mostly connected to the intermediate cingulate cortex. rsFC confirms this dichotomy (Nanetti et al., 2009; Taylor et al., 2008 and present study).

Subcortical functional connectivity of the insula

Our rsFC data also show functional connections between the thalamus and anterior insula, within the anterior network, while the dorsal insula and the posterior network do not seem to be functionally associated with the thalamus. Studies of primate anatomy reveal distinct regions of the insula that have different patterns of thalamic projections (Jones and Burton 1976). In addition, the whole parainsular field displays a strong projection to the medial geniculate body (Burton and Jones 1976). Furthermore, the insula receives projections from several thalamic cell groups, such as from the centromedian, ventroposterior medial, inferior and lateral nuclei, and projects back to the ventral medial, the ventroposterior, the parafascicularis and the dorsalis nuclei, as shown in monkeys (Augustine 1996; Flynn et al. 1999). Thalamic projections to the insula are also region-specific, i.e. the ventroposterior medial and centromedian nuclei project to the anterior insula, whereas the medial geniculate nucleus projects to the posterior insula (Guldin and Markowitsch, 1984). In turn, the dysgranular ventral

anterior insula projects to the ventroposterior and ventrolateral thalamic nuclei, whereas the granular dorsal posterior insula is connected to the posteromedial and ventroposterior inferior thalamic nuclei (Clasca et al., 1997).

Some apparent discrepancies exist between these reports and our rsFC data: our methodology does not show any functional connections between the posterior insula and the thalamus. This might be due to the different levels of sensitivities of the two methodologies. Interestingly, the expected pattern of thalamic connections is well replicated by the subcortical anticorrelations (Table 2); however, the direct interpretation of anticorrelations is still being debated. On the other hand, FC is indicated between both divisions of the insula and the basal ganglia, while reports of anatomical connectivity between the insula and basal ganglia are rare (Augustine, 1996; Flynn et al., 1999). These data underscore that there may not be a one-to-one relationship between FC and anatomical connectivity, but they also highlight the fact that anatomical tract-tracing usually indicates direct pathways whereas FC may also reflect multisynaptic pathways in a common network.

Lateralization of the insula and its connections

The insular lobes of the two sides have slightly different developmental sequences: the right lobe ceases growth earlier than the left, whereas the left lobe has a larger surface than the right, especially in humans (Carpenter, 1991). Interhemispheric and interindividual variability has also been reported for the insula in sections stained for cytochrome oxidase and for NADPH-d and acetylcholine esterase (Rivier and Clarke, 1997). Our results suggest that the insulae of the two sides also have different patterns of FC. The SN (anterior cluster) is frankly lateralized on the right, displays stronger connections especially with the right AI, rACC and several subcortical structures such as brainstem, pons and thalamus.

The visuomotor integration network (posterior cluster) displays only a mild right lateralization for the connections with the superior temporal cortex and the occipital cortex.

These data are in line with the connectivity hypothesis formulated by Craig (2002, 2005, 2008) and support the idea of the SN (Menon and Uddin, 2010; Seeley et al., 2007) and the role of the right insular cortex as a pivotal region in the attentional systems of the brain (Sridharan et al., 2008; Nelson et al., 2010).

Functional role of the insula

The insula represents an important site of multimodal convergence. It is involved in gustatory, visceral sensation and visceral motor responses (Penfield and Faulk, 1955) and in the processing of vestibular function, attention, pain, emotion, and verbal, motor, and musical information, in addition to olfactory, visual, auditory and tactile data (Craig, 2002, 2003). The insula has also been implicated in processing recall-generated sadness, anger, fear, disgust, happiness and aversive emotional stimuli (Nagai et al., 2007), and is associated with visual–tactile and auditory–visual integration.

According to Craig (2002), interoceptive information (visceral sensation) is conveyed to the posterior insular cortex, and integrated in the right AI. Affective and emotional components are conveyed to the insula via reciprocal connections with the amygdala and the nucleus accumbens (Reynolds and Zahm, 2005), and with the orbitofrontal cortex (Ongur and Price, 2000). Therefore, the insular cortex is strategically located for receiving and integrating both positive and aversive interoceptive information (Paulus and Stein, 2006). Our results support the idea that the dorsal posterior insula is functionally connected to sensory areas, thus bringing visceral sensation to the posterior network, whereas the ventral anterior is mostly connected to the limbic system, thus bringing emotional aspects to the anterior network. Thus, the insula integrates interoception and exteroception with emotion and memory giving the perception of self and of how the self feels (Bonthius et al., 2005; Craig, 2010).

The insula has also been implicated in a SN, which includes the dorsolateral prefrontal cortex and the anterior insula, and is jointly referred as the fronto-insular cortex (Menon and Uddin, 2010; Seeley et al., 2007; Sridharan et al. 2008). A fundamental issue is how this network, which has been identified in the resting state, operates during task performance. According to Dosenbach et al. (Dosenbach et al., 2007; Nelson et al., 2010), brain structures which participate in this SN facilitate multiple cognitive functions, such as initiation, maintenance and adjustment of attention; moreover, connections with the frontal cortex and limbic regions, subjective aspects, such as cognitive, homeostatic or emotional functions, are added to this salient network. According to several authors, then, the SN plays a key role in the hierarchical initiation of cognitive control signals.

The fronto-insular cortex and rACC, shown in our study as being strongly interconnected with the functional anterior network, share significant topographic, reciprocal connectivity, and can integrate information from several brain regions. Taken together, these cortical regions can moderate arousal during cognitively demanding tasks. The rostral fronto-insular cortex, in particular, plays a critical role in the interoceptive awareness of both stimulus-induced and stimulus-independent changes in homeostatic states. Information is relayed from the anterior insular cortex to the rACC: this relationship is likely to relate the internal body state to attention and planning (Corbetta and Shulman, 2002; Craig, 2002, 2010; Dosenbach et al., 2006, 2007; Fox et al., 2006; Karnath and Baier, 2010; Menon and Uddin, 2010; Seeley et al., 2007; Sridharan et al., 2008; Taylor et al., 2008).

The special relationship between the human fronto-insular cortex and the anterior cingulate cortex is reflected in a specialized class of neurons, the so-called von Economo neurons (VENs) that have distinctive anatomical and functional features for facilitating this network. VENs are large bipolar neurons located in infragranular layers of the frontoinsular and anterior cingulate cortex of humans and chimpanzees (Allman et al., 2010). Anatomical tract-tracing studies showed that VENs in the anterior cingulate cortex send their axons through the white matter of the cingulum to other areas of the brain (Nimchinsky et al., 1995). Allman et al. (2005, 2010) proposed that "the function of the VENs may be to provide a rapid relay to other parts of the brain of a simple signal derived from information processed within fronto-insular and Anterior Cingulate Cortex."

To sum up, the fronto-insular cortex has a powerful causal influence on the rACC. The functional anterior network could be the substrate for this influence, suggesting a causal, and potentially critical, role for the rostral fronto-insular cortex in cognitive control. According to several authors, a fundamental mechanism underlying such control would be a transient signal from the rostral fronto-insular cortex, which engages the brain's attentional, working memory and higher-order control processes, while disengaging other systems that are not task-relevant.

The posterior insula reportedly plays a role in auditory processing, supporting the hypothesis that it represents mainly a sensory area, as suggested by its cytoarchitectural features (Bamiou et al., 2003). Our rsFC data also document that the posterior insula has widespread and well-developed connections with the auditory cortex (Flynn et al., 1999).

Conclusions

Resting brain studies confirm and extend the notion that the human insula can be divided into two functionally distinct areas, the anterior and the posterior, which belong to two different functional networks, one related to the limbic functions and the other related to sensorimotor integration. We have described the two networks at cortical and subcortical levels, extending the already known involvement of the insular cortex in brain connectivity. Moreover, we have shown that the two patterns of network activation are lateralized,

more remarkably the anteroventral salience network on the right side. Analysis of such networks in patients could reveal altered patterns of connectivity that may either underlie, and predispose individuals to, or be the result and sign of specific neuropsychiatric diseases.

Acknowledgments

We wish to thank all the subjects who participated in this study. This work was supported by Regione Piemonte, bando Scienze Umane e Sociali 2008, L.R. n. 4/2006 and was submitted in partial fulfillment of the requirements for the doctoral degree (FC).

References

Achard, S., Salvador, R., Whitcher, B., Suckling, J., Bullmore, E., 2006. A resilient, low-frequency, small-world human brain functional network with highly connected association cortical hubs. J. Neurosci. 26, 63–72.

Aggleton, J.P., Burton, M.J., Passingham, R.E., 1980. Cortical and subcortical afferents to the amygdala of the rhesus monkey (*Macaca mulatta*). Brain Res. 190, 347–368.

Allman, J.M., Watson, K.K., Tetreault, N.A., Hakeem, A.Y., 2005. Intuition and autism: a possible role for Von Economo neurons. Trends Cogn. Sci. 9, 367–373.

Allman, J.M., Tetreault, N.A., Hakeem, A.Y., Manaye, K.F., Semendeferi, K., Erwin, J.M., Park, S., Goubert, V., Hof, P.R., 2010. The von Economo neurons in frontoinsular and anterior cingulate cortex in great apes and humans. Brain Struct. Funct. 214, 495–517.

Augustine, J.R., 1985. The insular lobe in primates including humans. Neurol. Res. 7, 2–10.

Augustine, J.R., 1996. Circuitry and functional aspects of the insular lobe in primates including humans. Brain Res. Brain Res. Rev. 22, 229–244.

Bamiou, D.E., Musiek, F.E., Luxon, L.M., 2003. The insula (Island of Reil) and its role in auditory processing. Literature review. Brain Res. Brain Res. Rev. 42, 143–154.

Bandettini, P.A., Bullmore, E., 2008. Endogenous oscillations and networks in functional magnetic resonance imaging. Hum. Brain Mapp. 29, 737–739.

Beckmann, C.F., DeLuca, M., Devlin, J.T., Smith, S.M., 2005. Investigations into resting-state connectivity using independent component analysis. Philos. Trans. R. Soc. Lond. B Biol. Sci. 360, 1001–1013.

Bezdek, J.C., Ehrlich, R., Full, W., 1984. FCM: the fuzzy c-means clustering algorithm. Comput. Geosci. 10, 191–203.

Bingham, W.C., Burke, H.R., Murray, S., 1966. Raven's progressive matrices: construct validity. J. Psychol. 62, 205–209.

Birn, R.M., Diamond, J.B., Smith, M.A., Bandettini, P.A., 2006. Separating respiratory-variation-related fluctuations from neuronal-activity-related fluctuations in fMRI. Neuroimage 31, 1536–1548.

Birn, R.M., Smith, M.A., Jones, T.B., Bandettini, P.A., 2008. The respiration response function: the temporal dynamics of fMRI signal fluctuations related to changes in respiration. Neuroimage 40, 644–654.

Biswal, B., Yetkin, F.Z., Haughton, V.M., Hyde, J.S., 1995. Functional connectivity in the motor cortex of resting human brain using echo-planar MRI. Magn. Reson. Med. 34, 537–541.

Bonthius, D.J., Solodkin, A., Van Hoesen, G.W., 2005. Pathology of the insular cortex in Alzheimer disease depends on cortical architecture. J. Neuropathol. Exp. Neurol. 64, 910–922.

Brooks, J.C., Zambreanu, L., Godinez, A., Craig, A.D., Tracey, I., 2005. Somatotopic organisation of the human insula to painful heat studied with high resolution functional imaging. Neuroimage 27, 201–209.

Burton, H., Jones, E.G., 1976. The posterior thalamic region and its cortical projection in New World and Old World monkeys. J. Comp. Neurol. 168, 249–301.

Carpenter, M.B., 1991. Core Text of Neuroanatomy. Williams & Wilkins, Baltimore.

Cauda, F., Geminiani, G., D'Agata, F., Sacco, K., Duca, S., Bagshaw, A.P., Cavanna, A.E., 2010a. Functional connectivity of the posteromedial cortex. PLoS ONE 5.

Cauda, F., Giuliano, G., Federico, D., Sergio, D., Katiuscia, S., 2010b. Discovering the somatotopic organization of the motor areas of the medial wall using low-frequency bold fluctuations. Hum Brain Mapp. Sep 2. [Epub ahead of print] PubMed PMID: 20814959.

Charter, R.A., 2001. Testing the equality of two or more split-half reliability coefficients. Psychol. Rep. 88, 844–846.

Clasca, F., Llamas, A., Reinoso-Suarez, F., 1997. Insular cortex and neighboring fields in the cat: a redefinition based on cortical microarchitecture and connections with the thalamus. J. Comp. Neurol. 384, 456–482.

Cole, L.J., Farrell, M.J., Duff, E.P., Barber, J.B., Egan, G.F., Gibson, S.J., 2006. Pain sensitivity and fMRI pain-related brain activity in Alzheimer's disease. Brain 129, 2957–2965.

Corbetta, M., Shulman, G.L., 2002. Control of goal-directed and stimulus-driven attention in the brain. Nat. Rev. Neurosci. 3, 201–215.

Craig, A.D., 2002. How do you feel? Interoception: the sense of the physiological condition of the body. Nat. Rev. Neurosci. 3, 655–666.

Craig, A.D., 2003. Interoception: the sense of the physiological condition of the body. Curr. Opin. Neurobiol. 13, 500–505.

Craig, A.D., 2004. Human feelings: why are some more aware than others? Trends Cogn. Sci. 8, 239–241.

Craig, A.D., 2005. Forebrain emotional asymmetry: a neuroanatomical basis? Trends Cogn. Sci. 9, 566–571.

Craig, A.D., 2008. Interoception and emotion: a neuroanatomical perspective. In: Lewis, M.J., Haviland-Jones, J.M., Barrett, L.F. (Eds.), Handbook of Emotions. Guilford Press, New York; London, pp. 272–288.

Craig, A.D., 2010. The sentient self. Brain Struct. Funct. 214, 563–577.

Critchley, H.D., Wiens, S., Rotshtein, P., Ohman, A., Dolan, R.J., 2004. Neural systems supporting interoceptive awareness. Nat. Neurosci. 7, 189–195.

Damoiseaux, J.S., Rombouts, S.A., Barkhof, F., Scheltens, P., Stam, C.J., Smith, S.M., Beckmann, C.F., 2006. Consistent resting-state networks across healthy subjects. Proc. Natl Acad. Sci. USA 103, 13848–13853.

Damoiseaux, J.S., Beckmann, C.F., Arigita, E.J., Barkhof, F., Scheltens, P., Stam, C.J., Smith, S.M., Rombouts, S.A., 2008. Reduced resting-state brain activity in the "default network" in normal aging. Cereb. Cortex 18, 1856–1864.

De Luca, M., Beckmann, C.F., De Stefano, N., Matthews, P.M., Smith, S.M., 2006. fMRI resting state networks define distinct modes of long-distance interactions in the human brain. Neuroimage 29, 1359–1367.

Devinsky, O., Morrell, M.J., Vogt, B.A., 1995. Contributions of anterior cingulate cortex to behaviour. Brain 118, 279–306.

Dosenbach, N.U., Visscher, K.M., Palmer, E.D., Miezin, F.M., Wenger, K.K., Kang, H.C., Burgund, E.D., Grimes, A.L., Schlaggar, B.L., Petersen, S.E., 2006. A core system for the implementation of task sets. Neuron 50, 799–812.

Dosenbach, N.U., Fair, D.A., Miezin, F.M., Cohen, A.L., Wenger, K.K., Dosenbach, R.A., Fox, M.D., Snyder, A.Z., Vincent, J.L., Raichle, M.E., Schlaggar, B.L., Petersen, S.E., 2007. Distinct brain networks for adaptive and stable task control in humans. Proc. Natl Acad. Sci. USA 104, 11073–11078.

Fadili, M.J., Ruan, S., Bloyet, D., Mazoyer, B., 2000. A multistep unsupervised fuzzy clustering analysis of fMRI time series. Hum. Brain Mapp. 10, 160–178.

Fadili, M.J., Ruan, S., Bloyet, D., Mazoyer, B., 2001. On the number of clusters and the fuzziness index for unsupervised FCA application to BOLD fMRI time series. Med. Image Anal. 5, 55–67.

Fair, D.A., Cohen, A.L., Dosenbach, N.U., Church, J.A., Miezin, F.M., Barch, D.M., Raichle, M.E., Petersen, S.E., Schlaggar, B.L., 2008. The maturing architecture of the brain's default network. Proc. Natl Acad. Sci. USA 105, 4028–4032.

Flynn, F.G., Benson, D.F., Ardila, A., 1999. Anatomy of insula – functional and clinical correlates. Aphasiology 13, 55–78.

Folstein, M.F., Folstein, S.E., McHugh, P.R., 1975. Mini-mental state. A practical method for grading the cognitive state of patients for the clinician. J. Psychiatr. Res. 12, 189–198.

Forman, S.D., Cohen, J.D., Fitzgerald, M., Eddy, W.F., Mintun, M.A., Noll, D.C., 1995. Improved assessment of significant activation in functional magnetic resonance imaging (fMRI): use of a cluster-size threshold. Magn. Reson. Med. 33, 636–647.

Fox, M.D., Snyder, A.Z., Vincent, J.L., Corbetta, M., Van Essen, D.C., Raichle, M.E., 2005. The human brain is intrinsically organized into dynamic, anticorrelated functional networks. Proc. Natl Acad. Sci. USA 102, 9673–9678.

Fox, M.D., Corbetta, M., Snyder, A.Z., Vincent, J.L., Raichle, M.E., 2006. Spontaneous neuronal activity distinguishes human dorsal and ventral attention systems. Proc. Natl Acad. Sci. USA 103, 10046–10051.

Fox, M.D., Raichle, M.E., 2007. Spontaneous fluctuations in brain activity observed with functional magnetic resonance imaging. Nat. Rev. Neurosci. 8, 700–711.

Fox, M.D., Zhang, D., Snyder, A.Z., Raichle, M.E., 2009. The global signal and observed anticorrelated resting state brain networks. J. Neurophysiol. 101, 3270–3283.

Fransson, P., 2006. How default is the default mode of brain function? Further evidence from intrinsic BOLD signal fluctuations. Neuropsychologia 44, 2836–2845.

Friston, K.J., Frith, C.D., Liddle, P.F., Frackowiak, R.S., 1993. Functional connectivity: the principal-component analysis of large (PET) data sets. J. Cereb. Blood Flow Metab. 13, 5–14.

Friston, K.J., 2007. Statistical Parametric Mapping: the Analysis of Functional Brain Images. Academic, London.

Genovese, C.R., Lazar, N.A., Nichols, T., 2002. Thresholding of statistical maps in functional neuroimaging using the false discovery rate. Neuroimage 15, 870–878.

Ghosh, A., Rho, Y., McIntosh, A.R., Kotter, R., Jirsa, V.K., 2008. Cortical network dynamics with time delays reveals functional connectivity in the resting brain. Cogn. Neurodyn. 2, 115–120.

Goebel, R., Esposito, F., Formisano, E., 2006. Analysis of functional image analysis contest (FIAC) data with brainvoyager QX: from single-subject to cortically aligned group general linear model analysis and self-organizing group independent component analysis. Hum. Brain Mapp. 27, 392–401.

Golay, X., Kollias, S., Stoll, G., Meier, D., Valavanis, A., Boesiger, P., 1998. A new correlation-based fuzzy logic clustering algorithm for fMRI. Magn. Reson. Med. 40, 249–260.

Greicius, M.D., Krasnow, B., Reiss, A.L., Menon, V., 2003. Functional connectivity in the resting brain: a network analysis of the default mode hypothesis. Proc. Natl Acad. Sci. USA 100, 253–258.

Greicius, M.D., Supekar, K., Menon, V., Dougherty, R.F., 2009. Resting-state functional connectivity reflects structural connectivity in the default mode network. Cereb. Cortex 19, 72–78.

Guldin, W.O., Markowitsch, H.J., 1984. Cortical and thalamic afferent connections of the insular and adjacent cortex of the cat. J. Comp. Neurol. 229, 393–418.

Hagmann, P., Cammoun, L., Gigandet, X., Meuli, R., Honey, C.J., Wedeen, V.J., Sporns, O., 2008. Mapping the structural core of human cerebral cortex. PLoS Biol. 6, e159.

Hampson, M., Peterson, B.S., Skudlarski, P., Gatenby, J.C., Gore, J.C., 2002. Detection of functional connectivity using temporal correlations in MR images. Hum. Brain Mapp. 15, 247–262.

Horwitz, B., 2003. The elusive concept of brain connectivity. Neuroimage 19, 466–470.
Johansen-Berg, H., Behrens, T.E., Robson, M.D., Drobnjak, I., Rushworth, M.F., Brady, J.M., Smith, S.M., Higham, D.J., Matthews, P.M., 2004. Changes in connectivity profiles define functionally distinct regions in human medial frontal cortex. Proc. Natl Acad. Sci. USA 101, 13335–13340.
Hughes, C.P., Berg, L., Danziger, W.L., Coben, L.A., Martin, R.L., 1982. A new clinical scale for the staging of dementia. Br. J. Psychiatry 140, 566–572.
Jones, E.G., Burton, H., 1976. Areal differences in the laminar distribution of thalamic afferents in cortical fields of the insular, parietal and temporal regions of primates. J. Comp. Neurol. 168, 197–247.
Karnath, H.O., Baier, B., 2010. Right insula for our sense of limb ownership and self-awareness of actions. Brain Struct. Funct. 214, 411–417.
Kim, J.H., Lee, J.M., Jo, H.J., Kim, S.H., Lee, J.H., Kim, S.T., Seo, S.W., Cox, R.W., Na, D.L., Kim, S.I., Saad, Z.S., 2009. Defining functional SMA and pre-SMA subregions in human MFC using resting state fMRI: functional connectivity-based parcellation method. Neuroimage 49, 2375–2386.
Kurth, F., Eickhoff, S.B., Schleicher, A., Hoemke, L., Zilles, K., Amunts, K., 2010a. Cytoarchitecture and probabilistic maps of the human posterior insular cortex. Cereb. Cortex 20, 1448–1461.
Kurth, F., Zilles, K., Fox, P.T., Laird, A.R., Eickhoff, S.B., 2010b. A link between the systems: functional differentiation and integration within the human insula revealed by meta-analysis. Brain Struct. Funct. 214, 519–534.
Lamm, C., Singer, T., 2010. The role of anterior insular cortex in social emotions. Brain Struct. Funct. 214 (5–6), 579–591.
Margulies, D.S., Kelly, A.M., Uddin, L.Q., Biswal, B.B., Castellanos, F.X., Milham, M.P., 2007. Mapping the functional connectivity of anterior cingulate cortex. Neuroimage 37, 579–588.
Menon, V., Uddin, L.Q., 2010. Saliency, switching, attention and control: a network model of insula function. Brain Struct. Funct. 214, 655–667.
Mesulam, M.M., Mufson, E.J., 1982a. Insula of the old world monkey. I. Architectonics in the insulo-orbito-temporal component of the paralimbic brain. J. Comp. Neurol. 212, 1–22.
Mesulam, M.M., Mufson, E.J., 1982b. Insula of the old world monkey. III: efferent cortical output and comments on function. J. Comp. Neurol. 212, 38–52.
Miezin, F.M., Maccotta, L., Ollinger, J.M., Petersen, S.E., Buckner, R.L., 2000. Characterizing the hemodynamic response: effects of presentation rate, sampling procedure, and the possibility of ordering brain activity based on relative timing. Neuroimage 11, 735–759.
Moller, U., Ligges, M., Georgiewa, P., Grunling, C., Kaiser, W.A., Witte, H., Blanz, B., 2002. How to avoid spurious cluster validation? A methodological investigation on simulated and fMRI data. Neuroimage 17, 431–446.
Mufson, E.J., Mesulam, M.M., 1982. Insula of the old world monkey. II: afferent cortical input and comments on the claustrum. J. Comp. Neurol. 212, 23–37.
Mutschler, I., Wieckhorst, B., Kowalevski, S., Derix, J., Wentlandt, J., Schulze-Bonhage, A., et al., 2009. Functional organization of the human anterior insular cortex. Neurosci. Lett. 457 (2), 66–70.
Nagai, M., Kishi, K., Kato, S., 2007. Insular cortex and neuropsychiatric disorders: a review of recent literature. Eur. Psychiatry 22, 387–394.
Naidich, T.P., Kang, E., Fatterpekar, G.M., Delman, B.N., Gultekin, S.H., Wolfe, D., Ortiz, O., Yousry, I., Weismann, M., Yousry, T.A., 2004. The insula: anatomic study and MR imaging display at 1.5 T. AJNR. Am. J. Neuroradiol. 25, 222–232.
Nanetti, L., Cerliani, L., Gazzola, V., Renken, R., Keysers, C., 2009. Group analyses of connectivity-based cortical parcellation using repeated k-means clustering. Neuroimage 47, 1666–1677.
Napadow, V., Dhond, R., Conti, G., Makris, N., Brown, E.N., Barbieri, R., 2008. Brain correlates of autonomic modulation: combining heart rate variability with fMRI. Neuroimage 42, 169–177.
Nelson, S.M., Dosenbach, N.U., Cohen, A.L., Wheeler, M.E., Schlaggar, B.L., Petersen, S.E., 2010. Role of the anterior insula in task-level control and focal attention. Brain Struct. Funct. 214, 669–680.
Nimchinsky, E.A., Vogt, B.A., Morrison, J.H., Hof, P.R., 1995. Spindle neurons of the human anterior cingulate cortex. J. Comp. Neurol. 355, 27–37.
Novelli, G., Papagno, C., Capitani, E., Laiacona, M., Cappa, S.F., Vallar, G., 1986a. Tre test clinici di memoria verbale a lungo termine. Taratura su soggetti normali. Archivio di Psicologia. Neurol. Psychiatry 47, 278–296.
Novelli, G., Papagno, C., Capitani, E., Laiacona, M., Cappa, S.F., Vallar, G., 1986b. Tre test clinici di ricerca e produzione lessicale. Taratura su soggetti normali. Archivio di Psicologia. Neurol. Psychiatry 47, 477–506.
Olausson, H., Charron, J., Marchand, S., Villemure, C., Strigo, I.A., Bushnell, M.C., 2005. Feelings of warmth correlate with neural activity in right anterior insular cortex. Neurosci. Lett. 389, 1–5.
Ongur, D., Price, J.L., 2000. The organization of networks within the orbital and medial prefrontal cortex of rats, monkeys and humans. Cereb. Cortex 10, 206–219.
Osterrieth, P.A., 1944. Le test de copie d'une figure complex: Contribution a l'etude de la perception et de la memoire [The Complex Figure Test: Contribution to the study of perception and memory]. Arch. Psychol. 28, 1021–1034.
Ostrowsky, K., Magnin, M., Ryvlin, P., Isnard, J., Guenot, M., Mauguiere, F., 2002. Representation of pain and somatic sensation in the human insula: a study of responses to direct electrical cortical stimulation. Cereb. Cortex 12, 376–385.
Paulus, M.P., Stein, M.B., 2006. An insular view of anxiety. Biol. Psychiatry 60, 383–387.
Penfield, W., Faulk, M.E., 1955. The insula; further observations on its function. Brain 78, 445–470.
Pollatos, O., Schandry, R., Auer, D.P., Kaufmann, C., 2007. Brain structures mediating cardiovascular arousal and interoceptive awareness. Brain Res. 1141, 178–187.
Reil, J.C., 1809. Die sylvische Grube. Arch. Physiol. Halle 9, 195–208.
Reitan, R.M., 1955. The relation of the trail making test to organic brain damage. J. Consult. Psychol. 19, 393–394.
Rey, A., 1958. L'examen clinique en psychologie. Presses Universitaires de France, Paris.
Reynolds, S.M., Zahm, D.S., 2005. Specificity in the projections of prefrontal and insular cortex to ventral striatopallidum and the extended amygdala. J. Neurosci. 25, 11757–11767.
Rivier, F., Clarke, S., 1997. Cytochrome oxidase, acetylcholinesterase, and NADPH-diaphorase staining in human supratemporal and insular cortex: evidence for multiple auditory areas. Neuroimage 6, 288–304.
Schweinhardt, P., Glynn, C., Brooks, J., McQuay, H., Jack, T., Chessell, I., Bountra, C., Tracey, I., 2006. An fMRI study of cerebral processing of brush-evoked allodynia in neuropathic pain patients. Neuroimage 32, 256–265.
Seeley, W.W., Menon, V., Schatzberg, A.F., Keller, J., Glover, G.H., Kenna, H., Reiss, A.L., Greicius, M.D., 2007. Dissociable intrinsic connectivity networks for salience processing and executive control. J. Neurosci. 27, 2349–2356.
Shehzad, Z., Kelly, A.M., Reiss, P.T., Gee, D.G., Gotimer, K., Uddin, L.Q., Lee, S.H., Margulies, D.S., Roy, A.K., Biswal, B.B., Petkova, E., Castellanos, F.X., Milham, M.P., 2009. The resting brain: unconstrained yet reliable. Cereb. Cortex.
Smolders, A., De Martino, F., Staeren, N., Scheunders, P., Sijbers, J., Goebel, R., Formisano, E., 2007. Dissecting cognitive stages with time-resolved fMRI data: a comparison of fuzzy clustering and independent component analysis. Magn. Reson. Imaging 25, 860–868.
Sridharan, D., Levitin, D.J., Menon, V., 2008. A critical role for the right fronto-insular cortex in switching between central-executive and default-mode networks. Proc. Natl Acad. Sci. USA 105, 12569–12574.
Stevens, M.C., Kiehl, K.A., Pearlson, G.D., Calhoun, V.D., 2007. Functional neural networks underlying response inhibition in adolescents and adults. Behav. Brain Res. 181, 12–22.
Talairach, J., Tournoux, P., 1988. Co-planar Stereotaxic Atlas of the Human Brain: 3-Dimensional Proportional System: an Approach to Cerebral Imaging. Thieme, Stuttgart.
Taylor, K.S., Seminowicz, D.A., Davis, K.D., 2008. Two systems of resting state connectivity between the insula and cingulate cortex. Hum. Brain Mapp. 30, 2731–2745.
Ture, U., Yasargil, D.C., Al-Mefty, O., Yasargil, M.G., 1999. Topographic anatomy of the insular region. J. Neurosurg. 90, 720–733.
Uddin, L.Q., Menon, V., 2009. The anterior insula in autism: under-connected and under-examined. Neurosci. Biobehav. Rev. 33, 1198–1203.
van Buuren, M., Gladwin, T.E., Zandbelt, B.B., van den Heuvel, M., Ramsey, N.F., Kahn, R.S., Vink, M., 2009. Cardiorespiratory effects on default-mode network activity as measured with fMRI. Hum. Brain Mapp. 30, 3031–3042.
Van Dijk, K.R., Hedden, T., Venkataraman, A., Evans, K.C., Lazar, S.W., Buckner, R.L., 2010. Intrinsic functional connectivity as a tool for human connectomics: theory, properties, and optimization. J. Neurophysiol. 103, 297–321.
Varnavas, G.G., Grand, W., 1999. The insular cortex: morphological and vascular anatomic characteristics. Neurosurgery 44, 127–136.
Vincent, J.L., Patel, G.H., Fox, M.D., Snyder, A.Z., Baker, J.T., Van Essen, D.C., Zempel, J.M., Snyder, L.H., Corbetta, M., Raichle, M.E., 2007. Intrinsic functional architecture in the anaesthetized monkey brain. Nature 447, 83–86.
Vogt, B.A., Pandya, D.N., Rosene, D.L., 1987. Cingulate cortex of the rhesus monkey: I. Cytoarchitecture and thalamic afferents. J. Comp. Neurol. 262, 256–270.
Vogt, B.A., 1993. Structural organization of cingulate cortex: areas, neurons and somatodendritic transmitter receptors. In: Vogt, B.A., Gabriel, M. (Eds.), Neurobiology of Cingulate Cortex and Limbic Thalamus: a Comprehensive Handbook. Mass, Birkhauser, Boston, pp. 19–70.
Vogt, B.A., Hof, P.R., Vogt, L.J., 2004. Cingulate gyrus. In: Paxinos, G., Mai, J.u.K. (Eds.), The Human Nervous System. Academic Press, San Diego, CA, pp. 915–949.
Weissenbacher, A., Kasess, C., Gerstl, F., Lanzenberger, R., Moser, E., Windischberger, C., 2009. Correlations and anticorrelations in resting-state functional connectivity MRI: a quantitative comparison of preprocessing strategies. Neuroimage 47, 1408–1416.
Woolrich, M.W., Ripley, B.D., Brady, M., Smith, S.M., 2001. Temporal autocorrelation in univariate linear modeling of FMRI data. Neuroimage 14, 1370–1386.
Zadeh, L.A., 1977. Fuzzy set and their application to pattern recognition and clustering analysis. In: Van Ryzin, J. (Ed.), Classification and Clustering: Proceedings of an Advanced Seminar Conducted by the Mathematics Research Center, the University of Wisconsin at Madison, May 3–5, 1976. Academic Press, New York, London, pp. 355–393.